POLITECNICO DI TORINO
Repository ISTITUZIONALE

Disaggregable Outage-Aware SNR Modeling under PDL Uncertainty for Optical Network Digital Twins

Original
Disaggregable Outage-Aware SNR Modeling under PDL Uncertainty for Optical Network Digital Twins / Miotto, E., Taricco, G., Nishizawa, H., D'Amico, A., Curri, V.. - In: IEEE OPEN JOURNAL OF THE COMMUNICATIONS SOCIETY. - ISSN 2644-125X. - (2026), pp. 1-25. [10.1109/ojcoms.2026.3741461]

Availability:
This version is available at: 11583/3016450 since: 2026-10-09T14:58:43Z

Publisher:
IEEE

Published
DOI:10.1109/ojcoms.2026.3741461

Terms of use:

This article is made available under terms and conditions as specified in the corresponding bibliographic description in the repository

Publisher copyright
IEEE postprint/Author's Accepted Manuscript

©2026 IEEE. Personal use of this material is permitted. Permission from IEEE must be obtained for all other uses, in any current or future media, including reprinting/republishing this material for advertising or promotional purposes, creating new collecting works, for resale or lists, or reuse of any copyrighted component of this work in other works.

(Article begins on next page)

26 November 2026

This article has been accepted for publication in IEEE Open Journal of the Communications Society. This is the author's version which has not been fully edited and content may change prior to final publication. Citation information: DOI 10.1109/OJCOMS.2026.3741461

IEEE Open Journal of the Communications Society

Received XX Month, XXXX; revised XX Month, XXXX; accepted XX Month, XXXX; Date of publication XX Month, XXXX; date of current version 11 January, 2024.

Digital Object Identifier 10.1109/OJCOMS.2024.011100

Disaggregable Outage-Aware SNR Modeling under PDL Uncertainty for Optical Network Digital Twins

ENRICO MIOTTO[1] *(Graduate Student Member, IEEE)*, **GIORGIO TARICCO** [1] *(Fellow, IEEE)*, **HIDEKI NISHIZAWA** [2] *(Senior Member, IEEE)*, **ANDREA D'AMICO** [3] *(Member, IEEE)*, **AND VITTORIO CURRI**[1] *(Fellow, IEEE)*

[1]Department of Electronics and Telecommunications, Politecnico di Torino, Turin, 10129, Italy
[2]NTT Network Innovation Laboratories, 1-1 Hikarinooka, Yokosuka, Kanagawa 239-0847, Japan
[3]NEC Laboratories America, 4 Independence Way, Princeton, New Jersey 08540, USA

CORRESPONDING AUTHOR: Enrico Miotto (e-mail: enrico.miotto@polito.it).

For this work, Politecnico di Torino has received funding from the EU Horizon project SENSEI (GA: 101189545).

ABSTRACT Polarization-dependent loss (PDL) makes the post-equalization signal-to-noise ratio (SNR) of a coherent optical lightpath stochastic, with an outage-relevant lower tail that depends on the longitudinal interleaving of PDL elements and amplified-spontaneous-emission (ASE) noise sources. Under a finite-hinge representation, the inverse-SNR is a weighted sum of correlated exponentials of a random walk, whose exact evaluation is too costly for repeated quality-of-transmission assessment in an optical network digital twin (ONDT), where physical-layer models are continuously combined with network data to predict transmission feasibility and support network operation. We model the PDL magnitude of each element through a Maxwell prior in dB and compare five efficient approximations: gamma moment matching, recursive moment-matched lognormal, correlated Fenton–Wilkinson lognormal, delta-cumulant log-skew-normal, and third-moment recursive log-skew-normal. Their descriptors can be accumulated element by element or exchanged as a constant-size moment state across vendor and operator domains, while allowing different PDL statistics in different network portions. Monte Carlo validation based on 10^9 realizations, with $N \in \{2, 10, 40\}$ and σ_{PDL} from 0.1 to 1.5 dB, shows that no approximation is uniformly best. In the practically relevant sub-1 dB range, the third-moment recursive log-skew-normal model is generally the most accurate global approximation and provides the best overall outage-tail prediction, with outage-probability errors typically within a few tenths of a decade and outage-quantile errors of about 0.2 dB or less. Realistic core–metro and metro–access examples further show that propagation direction, received optical power, and transceiver SNR jointly alter both the reference SNR and the distribution shape. The scope is limited to ASE-dominated links, independent per-element Maxwell priors, and ideal zero-forcing polarization equalization; Kerr nonlinear noise, non-ideal receivers, and correlated or telemetry-conditioned PDL models remain for future work.

INDEX TERMS outage estimation, optical communications, optical network digital twin, polarization-dependent loss, statistical margin assessment.

I. INTRODUCTION

OPTICAL transport networks are evolving from largely static infrastructures toward flexible, software-controlled systems in which spectrum, modulation format, baud rate, coding overhead, and delivered bit rate can be adapted to the demand and to the physical conditions of each lightpath [1], [2], [3], [4], [5], [6], [7]. In this context, an optical network digital twin (ONDT) can be viewed as a digital representation of the physical optical network that is maintained using network data and physical-layer models to estimate, predict, and evaluate network states for planning and operation [8]. Such a framework can provide

This work is licensed under a Creative Commons Attribution 4.0 License. For more information, see https://creativecommons.org/licenses/by/4.0/

This work is licensed under a Creative Commons Attribution 4.0 License. For more information, see https://creativecommons.org/licenses/by/4.0/

This article has been accepted for publication in IEEE Open Journal of the Communications Society. This is the author's version which has not been fully edited and content may change prior to final publication. Citation information: DOI 10.1109/OJCOMS.2026.3741461

the physical-layer awareness required to support increasingly flexible and automated optical-network operation [9]. This flexibility can substantially improve resource utilization, but only when the available quality of transmission (QoT) is estimated accurately. In particular, the signal-to-noise ratio (SNR) margin must be large enough to guarantee the required reliability while avoiding the capacity waste and network over-dimensioning produced by excessively conservative design rules [10], [11], [12].

Polarization-dependent loss (PDL) is especially challenging in this context because it is a non-unitary and stochastic impairment. Random polarization rotations along the fiber change the relative orientation between the propagating signal and the principal axes of the PDL elements, while signal and noise contributions encounter different portions of the PDL cascade. Consequently, the received SNR is a random variable whose lower tail, rather than only its nominal or average value, determines the probability of out-of-service (POOS) and the corresponding engineering margin [13], [14]. An exact finite-hinge description of the PDL-induced SNR distribution is available [15], but its recursive evaluation scales exponentially with the number of PDL elements and requires the PDL magnitude of every traversed device. Conversely, computationally efficient Gaussian or continuous-limit models are most reliable when the link contains many weak contributions and may not reproduce asymmetric outage tails in finite cascades with localized PDL.

The resulting gap is threefold. First, exact finite-hinge SNR statistics are not sufficiently scalable for repeated evaluation over many candidate lightpaths. Second, efficient approximations may lose accuracy precisely in the lower-SNR tail used for outage-aware margin assessment. Third, an open multi-vendor network rarely provides a complete characterization of every WSS port, frequency, and programmed attenuation, although these operating variables materially affect the inserted PDL. A practical optical network digital twin (ONDT) therefore needs a predictive statistical prior that is computationally efficient, composable along the path, and usable even when exhaustive per-device measurements are unavailable.

This work addresses these limitations by modeling the PDL magnitude introduced by each optical element as a Maxwell random variable, following the device-level variability observed across WSS ports, frequencies, and attenuation settings [16], [17], [18]. The Maxwell law is used here as a compact *per-element* prior and is distinct from the classical asymptotic Maxwell distribution of the total accumulated link PDL. In a fully disaggregated multi-vendor ONDT, its variance may be assigned separately to each vendor, device family, network portion, or operating class; the common variance used in part of the numerical validation is therefore a controlled baseline rather than an architectural restriction. The random polarization rotations between localized PDL elements are represented through the hinge-model abstraction adopted in [15], [19].

The statistical strategy is partly inspired by the wireless-communications treatment of random multipath channels, where tractable fading laws arise from sums of many randomly phased contributions. Taricco showed that convergence toward a circular complex Gaussian gain, and hence a Rayleigh amplitude, requires explicit conditions on the path gains and cannot be justified by an unqualified central-limit argument [20]. The random variable considered here is different; it is a positive, weighted sum of correlated exponential terms; but the same methodological lesson motivates retaining the finite-cascade structure and validating every approximation instead of imposing an asymptotic law a priori.

On this basis, we formulate the random inverse-SNR as a weighted sum of correlated exponentials and develop five computationally efficient semi-analytical approximations: gamma moment matching, recursive moment-matched lognormal, correlated Fenton–Wilkinson lognormal, delta-cumulant log-skew-normal, and third-moment recursive log-skew-normal. These distributions adapt tools originally developed for positive sums, correlated lognormal powers, and skewed data [21], [22]. Their parameters are expressed through quantities that can be accumulated element by element or passed as a compact moment state across administrative domains, enabling disaggregated execution and direct POOS evaluation without exposing every device detail. The models are first validated against the Monte Carlo framework developed for stochastic WSS PDL in [18] and are then applied to realistic core–metro and metro–access links with strongly non-uniform noise loading.

The contributions of this work are threefold. First, we derive recursive first-, second-, and third-order moments of the finite-hinge inverse-SNR and use them to construct low-complexity distributional approximations. Second, we express the recursions in backward and forward forms, including constant-size states that can be exchanged across administrative domains. Third, we compare five approximation families using both global distributional metrics and outage-oriented metrics over controlled Monte Carlo sweeps and four representative application cases with non-uniform noise loading. Section III and Table 1 position these contributions relative to the closest PDL-induced SNR models.

Unless explicitly identified as a total dual-polarization quantity, every signal and noise power used in the analytical model is defined for one recovered polarization tributary, i.e., one of the two recovered polarization axes.

The remainder of this paper is organized as follows. Section II discusses flexible optical networking, virtualization, ONDTs, and probabilistic margin assessment. Section III reviews the physical origin, monitoring, mitigation, statistics, and SNR impact of PDL, with emphasis on outage-aware models. Section IV introduces the stochastic per-element PDL and inverse-SNR model. Section V derives

This work is licensed under a Creative Commons Attribution 4.0 License. For more information, see https://creativecommons.org/licenses/by/4.0/

This article has been accepted for publication in IEEE Open Journal of the Communications Society. This is the author's version which has not been fully edited and content may change prior to final publication. Citation information: DOI 10.1109/OJCOMS.2026.3741461

the proposed distributional approximations, while Section VI describes their disaggregation and analytical outage evaluation. Section VII validates the models through Monte Carlo simulation. Section VIII presents representative application scenarios, and Section IX concludes the paper.

II. FLEXIBLE OPTICAL NETWORKS AND DIGITAL-TWIN-ENABLED MARGIN ASSESSMENT

Flexible-grid switching, programmable reconfigurable optical add–drop multiplexers, and bandwidth-variable transceivers can adapt the occupied spectrum, symbol rate, modulation format, coding overhead, and delivered bit rate to the demand and to the physical conditions of each lightpath [4], [5], [7]. These capabilities can improve spectral utilization and reduce the number of required lightpaths, but they also make network efficiency increasingly dependent on the accuracy with which the available QoT is assessed. For a rate-adaptive coherent transceiver, the SNR is not merely a monitoring quantity: together with the implementation penalty, it determines which transmission mode can be operated at the required reliability. Consequently, uncertainty in the available SNR must be covered by a margin. Such margins are indispensable for guaranteeing service over the network lifetime, but they also strand capacity and should therefore be no larger than required by the intended service guarantees [10]. The transition toward low- and near-zero-margin operation has accordingly been associated with accurate QoT estimation, continuous monitoring, characterization of performance fluctuations, and closed-loop control [11], [12].

In parallel, optical networks are evolving toward open, disaggregated, and virtualized infrastructures. Virtual optical networks and transport slices partition and compose physical ports, switching resources, spectrum, and lightpaths while providing isolation and service-specific control over a shared substrate. Device hypervisors, open data models, and software-defined orchestration have demonstrated the provisioning of such resources in partially disaggregated optical networks [23], [24], [25]. Disaggregation and virtualization are also central to the evolution and convergence of access and metro networks, where independent hardware and software evolution, infrastructure sharing, and automated service provisioning are expected to improve both agility and economy [26], [27]. Virtualization itself can be implemented without a digital twin; however, efficient embedding and QoT-assured operation of virtual optical resources require a trustworthy abstraction of the underlying transmission feasibility. In particular, the abstraction must expose not only nominal performance, but also the uncertainty relevant to the service-level agreement.

Optical network digital twins provide a natural framework for this physical-layer abstraction. Early digital-twin architectures for optical communications introduced dynamically updated models for transmission assessment, equipment configuration, and fault management [28]. GNPy showed how element-wise, vendor-neutral physical-layer models can support planning and management of open and disaggregated networks [8], while subsequent ONDT frameworks organized the problem around modeling, telemetry, and self-learning [29]. Measurement-informed physics-based, data-driven, and hybrid models can exploit coherent-transceiver telemetry to calibrate the virtual representation, although uncertainty, model interpretability, and rare extreme events remain essential challenges [30]. More recent work has extended this vision toward full-lifecycle management, autonomous control, and agentic closed loops in which telemetry provides the observations, the twin predicts network behavior, and control agents validate and execute actions [31], [32], [33]. Operator-driven ONDTs are also being investigated for all-photonics networks-as-a-service, including remote transponder control, rapid provisioning, physical-parameter estimation, and line-system calibration in distributed data-center infrastructures [34].

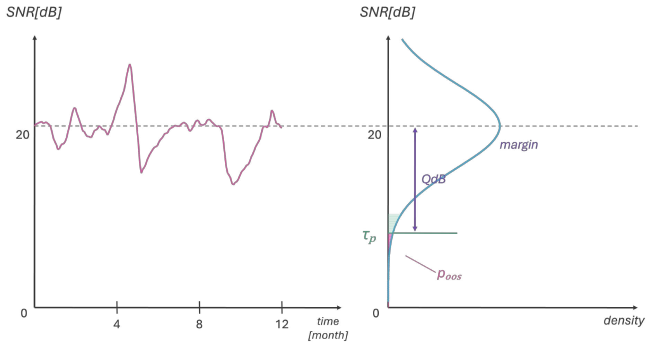

FIGURE 1. Statistical margin assessment of PDL-induced SNR for ONDT transmission modeling.

These developments make probabilistic margin assessment a necessary ONDT capability. For a stochastic physical-layer impairment, a prediction of the nominal or average SNR is insufficient: the relevant margin is determined by the lower-tail quantile of the SNR distribution associated with the target POOS. As illustrated in Fig. 1, a statistical margin can therefore be selected so that the probability of the instantaneous SNR falling below the operating threshold of the chosen transmission mode does not exceed the target POOS. This formulation preserves a quantifiable reliability guarantee while avoiding the systematic over-provisioning produced by worst-case assumptions. It motivates accurate and computationally efficient statistical models that can be repeatedly evaluated and updated within an ONDT.

III. FROM PDL PHYSICS TO OUTAGE-AWARE SNR MODELING

Polarization-dependent loss is the non-unitary polarization impairment produced when an optical element attenuates its two orthogonal principal states by different amounts. It is conventionally quantified by the ratio between the maximum and minimum transmitted powers over all input states of polarization. In present transport networks, the dom-

This work is licensed under a Creative Commons Attribution 4.0 License. For more information, see https://creativecommons.org/licenses/by/4.0/

This article has been accepted for publication in IEEE Open Journal of the Communications Society. This is the author's version which has not been fully edited and content may change prior to final publication. Citation information: DOI 10.1109/OJCOMS.2026.3741461

inant discrete sources are the wavelength-selective switches (WSSs) used in reconfigurable optical add–drop multiplexers (ROADMs) and, to a lesser extent, optical-amplifier subcomponents. WSSs integrate wavelength dispersion, switching, filtering, and variable optical attenuation; liquid-crystal-on-silicon implementations now dominate flexible-grid, high-port-count ROADMs, but their free-space and polarization-diversity optics can introduce non-negligible PDL [35], [36]. PDL and polarization-dependent gain have also long been associated with amplifier chains and components such as isolators [37], while localized fiber bends can generate polarization-dependent bend loss [38]. In the terrestrial-link regime considered here, the transmission fiber is typically weaker as a direct PDL source than the discrete devices [39], but its randomly distributed perturbations continuously rotate the state of polarization [40]. A terrestrial or metro lightpath is consequently well represented as a sequence of localized PDL "hinges" separated by approximately unitary, time-varying polarization rotations.

Several approaches have been proposed to reduce the resulting performance penalty. At the transceiver, multidimensional signaling can spread information across the two polarizations and reduce sensitivity to an unfavorable PDL orientation. Optimized four-dimensional SO(4) transforms and the New Spatially Balanced modulation were developed and experimentally validated for this purpose [41], [42]; polarization pairwise coding pursues a related objective with no coding-rate overhead and lower decoding complexity than space–time alternatives [43]. At the network-control level, large PDL anomalies can be detected from QoT fluctuations and mitigated by a closed loop that steers the operating point toward the best observed polarization condition [44]. These techniques improve resilience, but they do not remove the need to predict the residual probability that the instantaneous QoT falls below the operating threshold.

PDL has therefore also become an important monitoring target. Multi-day measurements on an installed 1800-km terrestrial WDM link showed variations on the scale of hours, correlation among nearby channels, and truncated rather than Maxwellian field distributions, consistent with only a few significant PDL elements [39]. The impact of PDL on the received OSNR has also been probed directly with coherent transmission experiments and then extended through Monte Carlo analysis to obtain a statistical penalty model [45]. Performance-statistics-based methods infer the PDL of deployed ROADMs from the mean and variance of transceiver-reported SNR distributions, reducing the uncertainty with respect to datasheet bounds and, in the extended formulation, reducing SNR margins on representative lightpaths [46], [47]. Other receiver-side techniques estimate both the value and longitudinal position of excessive PDL from polarization-resolved power profiles [48] or fit the complete per-polarization SNR PDF to localize and quantify multiple anomalous elements from a single receiver [49]. Such telemetry-driven techniques are valuable for established lightpaths and fault localization; the complementary problem addressed here is predictive: evaluating the SNR distribution, and especially its rare lower tail, before or during lightpath provisioning from a compact physical-layer description.

The statistics of the accumulated link PDL have been studied extensively. The Stokes- and Jones-space formalisms for concatenated birefringence and PDL established the vector representation and showed that a distributed impairment cannot in general be replaced by an end-of-line lumped loss without changing the transmission penalty [50]. For a very large number of weak, statistically independent contributions, the accumulated PDL magnitude expressed in dB approaches a Maxwell distribution and its mean-square value grows approximately linearly with distance [51]; an exact treatment beyond the small-PDL approximation was subsequently derived [52]. Installed terrestrial systems, however, may contain only a finite number of dominant components. For this regime, the hinge model gives exact distributions for link PDL and overall attenuation with fixed-magnitude discrete elements separated by random rotations [19], while a generalized finite-element PDF has been proposed for arbitrary numbers and strengths of PDL elements and shown to differ materially from the Maxwell law in practical cases [53]. Related outage studies have also used extreme-value threshold exceedances to extrapolate rare failures from finite simulated samples without postulating a global performance PDF [54]. These results are essential for characterizing the end-to-end PDL magnitude, but the present target is different: the margin is determined by the distribution of the received SNR, not by the PDL distribution alone.

The impact of PDL on transmission performance has already been extensively studied for intensity-modulation/direct-detection (IM/DD) systems, including the statistics of signal and noise accumulation, PDL-induced noise enhancement, dynamic gain equalization, and outage-oriented penalty assessment [55], [56], [57], [58]. The present work instead focuses on dual-polarization coherent systems, where the received complex field is processed by a polarization-demultiplexing MIMO equalizer.

In coherent systems, the same accumulated PDL can produce different SNR penalties because the signal and each amplified-spontaneous-emission (ASE) contribution traverse different subsets of the PDL cascade. Shtaif formulated the coherent polarization-multiplexed problem in terms of the signal and noise transfer matrices, showing why ideal DSP can restore the signal geometry but cannot in general undo the PDL-induced noise enhancement [13]. The reversed-channel method of Tao *et al.* reduced the computational cost of Monte Carlo analysis by propagating only the noise covariance and demonstrated that the longitudinal profiles of both PDL and ASE, rather than their accumulated values alone, determine the penalty [14]. A perturbative continuous-limit analysis subsequently obtained a Gaussian per-tributary SNR penalty in dB and closed expressions for its mean and variance for arbitrary PDL and ASE profiles [59]. WSS-

This work is licensed under a Creative Commons Attribution 4.0 License. For more information, see https://creativecommons.org/licenses/by/4.0/

This article has been accepted for publication in IEEE Open Journal of the Communications Society. This is the author's version which has not been fully edited and content may change prior to final publication. Citation information: DOI 10.1109/OJCOMS.2026.3741461

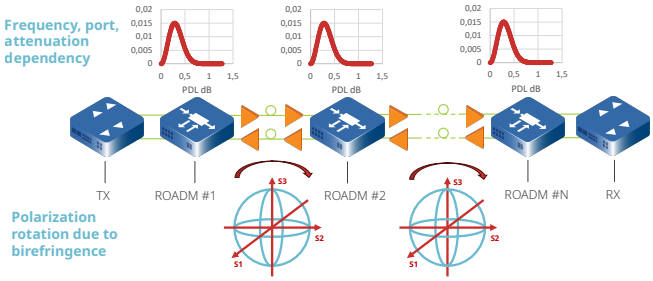

FIGURE 2. PDL-impaired optical-link scenario and the related stochastic effects caused by random choices of frequency, port, and attenuation and by random polarization rotation due to fiber birefringence.

based Monte Carlo analysis in a regional/metro topology likewise showed that reversing the order of the same noise and PDL resources can substantially change the penalty [16].

Further studies have refined this system-level viewpoint. Lumped and distributed PDL models can be related through an equivalent PDL value at a prescribed SNR penalty, but the equivalence depends on the link configuration [60]. Stochastic-differential-equation formulations have characterized the exact moments of the post-equalization noise-correlation matrix for continuously distributed PDL [61]. The impact of transceiver noise on PDL-induced outage has been quantified through generalized-mutual-information and threshold-exceedance analysis [62]. More recently, a deterministic SNR concatenation rule augmented by outage-dependent PDL factors was proposed to combine ASE noise, transceiver noise, Kerr nonlinearity, and PDL in a single QoT curve [63]. These approaches confirm that an outage margin must retain the relative positions of noise and PDL, the selected performance metric, and the receiver assumptions.

Gaussian modeling is attractive because it converts a target POOS directly into a quantile, and it has been used successfully in low-PDL experiments and disaggregated OSNR calculations. In particular, the disaggregated formulation of D'Amico *et al.* models the per-polarization OSNR with a truncated Gaussian and derives the distribution width and range from the deterministic PDL and ASE profiles [64]. Its domain of validity must nevertheless be kept explicit. The derivation of Dou *et al.* assumes a large number of nodes, a small PDL coefficient per node, and a finite accumulated squared PDL, and then retains the lowest perturbative order; the Gaussian SNR penalty follows in the additional small-penalty regime [59]. Finite-hinge-model links can instead exhibit irregular PDFs for very few elements and marked asymmetry when the individual PDL values are large [15]. Consequently, a Gaussian approximation can be accurate for many weak contributions and useful as a conservative low-PDL model, but it is not a universally reliable description of the outage-relevant tail when PDL is concentrated in a finite number of devices.

The interaction with Kerr nonlinearity adds a further layer of complexity. Numerical studies showed that realistic PDL can materially change outage probabilities even when its effect on the average Q-factor is small [65]. The Gaussian-noise framework has been extended to propagate the PDL-dependent nonlinear-noise covariance and estimate the corresponding outage probability much faster than repeated split-step simulations [66]. Nevertheless, the PDL–NLI interaction can broaden and skew the SNR distribution relative to the ASE-only prediction, and a reversed-channel model amended only with an additional Gaussian NLI variance may miss this change [67]. An analytical SDE/ODE treatment has more recently provided moments of the nonlinear-noise power and cross-polarization correlation in the presence of distributed PDL [68]. NLI is deliberately outside the scope of the present paper and is therefore its principal physical limitation. The analysis targets the ASE-dominated regime relevant to the short-reach, moderate-launch-power metro use cases considered in previous PDL studies [16], [18]; it should not be interpreted as a general claim that NLI is negligible in every metro lightpath. Extending the proposed approximations to power-dependent nonlinear-noise statistics is left for future work. We also recall that conservative and reasonably accurate margins can be obtained by treating NLI as an additive white Gaussian noise (AWGN) source concentrated at the receiver [69].

Chromatic dispersion is assumed to be compensated by the coherent receiver; residual dispersion and penalties caused by insufficient equalizer memory are not included. Polarization-mode dispersion is also outside the scalar hinge model. In conjunction with PDL, PMD can make the polarization response frequency dependent across the signal bandwidth [50] and can therefore change the post-equalization SNR distribution. Their joint treatment is outside the scope of this work.

A major analytical advance was recently achieved by deriving the exact marginal PDF of the PDL-induced SNR for a coherent dual-polarization link with discrete PDL hinges, distributed additive noise, and ideal zero-forcing equalization [15]. In the present work, ideal MIMO zero-forcing equalization is retained as a deliberate simplifying assumption to isolate the effect of the PDL-impaired channel on the post-equalization performance; extending the framework to MMSE and other implementation-aware MIMO equalizers is left for future work. The derivation transforms the random cascade into a sequence of nested recursive integrals and therefore captures finite-element, non-Gaussian behavior without invoking a central-limit approximation. It also provides the mathematical abstraction adopted in this paper. Its exactness, however, comes at a cost: the recursive evaluation inherits exponential complexity in the number of PDL devices, and each device must be characterized through its individual PDL magnitude. The method is fast for short cascades, including the range of three to eight ROADMs considered in many metro paths, but becomes unattractive for larger topologies, repeated what-if analyses, or ONDT optimization loops involving many candidate lightpaths.

This work is licensed under a Creative Commons Attribution 4.0 License. For more information, see https://creativecommons.org/licenses/by/4.0/

This article has been accepted for publication in IEEE Open Journal of the Communications Society. This is the author's version which has not been fully edited and content may change prior to final publication. Citation information: DOI 10.1109/OJCOMS.2026.3741461

Several works have explicitly connected PDL statistics to engineering margin. Operational rules often begin from a fixed or worst-case PDL allowance, which is simple to apply but can reserve capacity for very unlikely realizations. Nafta and Shtaif quantified the capacity-equivalent SNR penalty and the required margin at a prescribed outage probability, distinguishing an ultimate jointly coded limit from a more direct separate-tributary design [70]. Xie compared lumped and distributed PDL/ASE models for PDM-QPSK and found that a lumped emulator can significantly overestimate the penalty of a realistic distributed system [71]; together with the reversed-channel analyses, this confirms that a fixed end-to-end PDL margin cannot represent all longitudinal configurations. A metro-oriented study then treated the PDL magnitude inserted by each WSS as a random quantity, supported the need for this treatment through frequency-dependent measurements, and used Monte Carlo simulation to select a conservative POOS-based margin without imposing the maximum PDL at every node [18]. In that study, the uniform worst-case assignment reduced the admissible path by one ROADM relative to the stochastic reference, directly illustrating the cost of excessive conservatism. A subsequent closed-form model applied a central-limit approximation to the correlated inverse-SNR contributions and obtained experimentally conservative margins substantially below the corresponding OpenROADM recommendation [72]. This last approach is computationally efficient and important for ONDT use, but its Gaussian rationale is strongest in the many-small-contributions regime formalized by Dou *et al.*; finite, localized, and comparatively strong hinges motivate the more general approximation families studied here.

Table 1 summarizes the methodological differences between the present framework and the closest PDL-induced SNR models.

IV. SYSTEM MODEL

The purpose of this section is to establish the notation and stochastic link model used by the subsequent approximations. It defines the per-element PDL variable and normalized random gain, specifies the Maxwell prior and the required moments of the minus-logarithm of the normalized random gain, and derives the distributed-noise inverse-SNR representation.

A. PDL Variable, Hinge-Model Parameter, and Random Gain

Let X denote the PDL magnitude of a single optical element in dB. The corresponding linear PDL ratio is

$$\rho = 10^{X/10}. \tag{1}$$

Following the hinge-model parametrization of PDL statistics [15], [19], the PDL imbalance parameter is defined as

$$\gamma = \frac{\rho - 1}{\rho + 1} = \tanh(c_{\mathrm{dB}} X), \qquad c_{\mathrm{dB}} = \frac{\log(10)}{20}. \tag{2}$$

The parameter $\gamma \in [0, 1)$ determines the strength of the polarization-dependent attenuation induced by the device. In the exact hinge-model derivation, γ fixes the support and density of the single-device attenuation seen by a selected polarization tributary [15], [19]. In the normalized model used in this paper, the same imbalance parameter controls a positive multiplicative factor A, and we adopt the conditional representation

$$A \mid \gamma \sim \mathcal{U}(1 - \gamma, 1 + \gamma). \tag{3}$$

Thus, $0 < A < 2$ and $\mathbb{E}[A \mid \gamma] = 1$. This normalization preserves the essential property that PDL produces a random multiplicative gain with unit conditional mean, while the logarithmic variable $Z = -\log(A)$ has positive drift by Jensen's inequality whenever the element is non-degenerate. The additional randomness in (3) accounts for the random state of polarization impinging on the PDL element.

B. Per-Element Maxwell Model for PDL in dB

The PDL magnitude X of each element is modeled as a Maxwell random variable with scale parameter α_{M}:

$$f_X(x) = \sqrt{\frac{2}{\pi}} \frac{x^2}{\alpha_{\mathrm{M}}^3} \exp\left(-\frac{x^2}{2\alpha_{\mathrm{M}}^2}\right), \qquad x \geq 0. \tag{4}$$

If $\mathrm{Var}(X) = \sigma_{\mathrm{PDL}}^2$, where σ_{PDL} denotes the per-element PDL standard deviation in dB, then

$$\alpha_{\mathrm{M}}^2 = \frac{\sigma_{\mathrm{PDL}}^2}{3 - 8/\pi} = \frac{\pi \sigma_{\mathrm{PDL}}^2}{3\pi - 8}. \tag{5}$$

The use of a Maxwell law at the level of a single device in dB is a compact modeling choice motivated by experimental WSS characterizations. Those measurements show that the PDL is not represented by one deterministic device value: it varies across ports, spectral slices, and programmed attenuation, and its moments evolve with the operating point [16], [17]. Recent work on WDM networks with multirail amplifiers and 800ZR+ interfaces likewise draws the PDL of each LCoS-based element from a measured distribution and reports network-level differences relative to fixed per-element values [73]. This result supports a statistical per-element description; the Maxwell form used here is the compact one-parameter prior adopted in the metro-margin Monte Carlo framework of [18], specified through the per-element standard deviation σ_{PDL}. The resulting digital-twin descriptor avoids storing a separate experimental PDL histogram for every operating combination.

This per-element Maxwell assumption should not be confused with studies in which a Maxwellian law describes the total PDL accumulated after a cascade of randomly oriented elements [19], [39], [51], [52], [53]. Those works characterize the end-to-end PDL vector or magnitude; here, instead, X is the PDL of each individual component before the cascade is formed. As a first modeling step, and unless otherwise specified, we assume that all N elements share the same variance σ_{PDL}^2. A more detailed multi-vendor digital

This work is licensed under a Creative Commons Attribution 4.0 License. For more information, see https://creativecommons.org/licenses/by/4.0/

This article has been accepted for publication in IEEE Open Journal of the Communications Society. This is the author's version which has not been fully edited and content may change prior to final publication. Citation information: DOI 10.1109/OJCOMS.2026.3741461

TABLE 1. Positioning against the closest PDL-induced SNR models.

Approach	PDL regime and input	SNR evaluation and distinction from the present work
Reversed-channel Monte Carlo [14]	Specified longitudinal PDL and ASE profiles	Accelerates sampling by propagating noise covariance, but remains sample based and does not provide a constant-size analytical outage law.
Perturbative Gaussian model [59]	Many weak PDL contributions with prescribed longitudinal profiles	Gives Gaussian SNR-penalty moments in the small-PDL regime; finite strong hinges and asymmetric outage tails fall outside the approximation assumptions.
Disaggregated truncated Gaussian [64]	Deterministic PDL and ASE descriptors	Provides an efficient conservative OSNR distribution, whereas the present work compares non-Gaussian laws for random per-element PDL and finite cascades.
Stochastic WSS margin [18]	Maxwell-distributed per-WSS PDL supported by device measurements	Establishes a Monte Carlo POOS margin but does not derive a compact end-to-end distribution or an inter-domain recursion.
Exact finite-hinge PDF [15]	Arbitrary finite, localized hinges and distributed additive noise	Captures the non-Gaussian PDF exactly, but nested integration scales exponentially with N and requires each hinge magnitude.
Closed-form CLT margin [72]	Correlated inverse-SNR terms in the many-small-contribution regime	Is computationally efficient and conservative, but retains a Gaussian tail rather than testing alternative finite-cascade distribution families.
This work	Random, possibly heterogeneous per-element priors; finite hinges and ordered noise sources	Compares five positive laws, propagates up to three exact raw moments in $O(N)$ time and $O(1)$ memory, exchanges a five- or nine-entry state, and validates global and outage-tail errors.

twin could assign different Maxwell variances to different devices or equipment families.

Combining (2) and (4), the density of γ is

$$f_\gamma(g) = f_X\left(\frac{\operatorname{artanh}(g)}{c_{\mathrm{dB}}}\right)\frac{1}{c_{\mathrm{dB}}(1-g^2)}, \qquad 0<g<1. \tag{6}$$

The unconditional density of A is the mixture

$$f_A(a) = \int_{|a-1|}^{1} \frac{f_\gamma(g)}{2g}\,\mathrm{d}g, \qquad 0<a<2. \tag{7}$$

This density is symmetric around one, but the logarithmic variable $Z = -\log(A)$ is asymmetric and has positive mean.

C. Moments and Exponential Moments of $Z = -\log(A)$

Define

$$Z = -\log(A), \qquad \mu_Z = \mathbb{E}[Z], \qquad \sigma_Z^2 = \mathrm{Var}(Z). \tag{8}$$

For fixed γ,

$$\mathbb{E}[\log(A)\mid\gamma] = \frac{(1+\gamma)\log(1+\gamma)}{2\gamma} - \frac{(1-\gamma)\log(1-\gamma)}{2\gamma} - 1, \tag{9}$$

with the limit equal to zero as $\gamma\to 0$. Therefore

$$\mu_Z = -\mathbb{E}_\gamma\left[\mathbb{E}[\log(A)\mid\gamma]\right] > 0. \tag{10}$$

The variance and higher cumulants of Z can be obtained by integrating powers of $\log A$ over the conditional uniform distribution.

Several approximations below require exponential moments

$$\psi(s) = \mathbb{E}[e^{sZ}] = \mathbb{E}[A^{-s}]. \tag{11}$$

Conditionally on γ, for $s\neq 1$,

$$\psi(s\mid\gamma) = \frac{(1+\gamma)^{1-s} - (1-\gamma)^{1-s}}{2\gamma(1-s)}, \tag{12}$$

whereas

$$\psi(1\mid\gamma) = \frac{\log\left((1+\gamma)/(1-\gamma)\right)}{2\gamma} = \frac{\operatorname{artanh}(\gamma)}{\gamma}. \tag{13}$$

The unconditional $\psi(s)$ is obtained by averaging (12) over the Maxwell distribution of X. In an inhomogeneous link, the k-th element may have its own PDL law, and the corresponding quantities are denoted by $\mu_k = \mathbb{E}[Z_k]$, $v_k = \mathrm{Var}(Z_k)$, $\psi_k(s)$, and $K_k(s) = \log(\psi_k(s))$.

D. Distributed-Noise Link and Inverse-SNR Representation

Consider one recovered polarization tributary of a dual-polarization coherent link composed of N localized PDL elements and $N+1$ additive noise contributions. The receiver is assumed to apply ideal 2×2 MIMO zero-forcing equalization to recover the two polarization tributaries, consistently with the finite-hinge model adopted in [15]; the subsequent derivation refers to either recovered tributary individually. Consistently with the convention stated in Section I, p_s and every $p_{n,i}$ are powers on the considered single polarization axis; a total over both polarizations is used only when explicitly stated. Let p_s denote the launched signal power on the considered tributary, let $p_{n,1},\ldots,p_{n,N+1}$ denote the powers of the local noise contributions, and let A_k be the normalized random power-transfer factor introduced by the k-th PDL element. The signal traverses the complete cascade, whereas each noise contribution experiences only

This work is licensed under a Creative Commons Attribution 4.0 License. For more information, see https://creativecommons.org/licenses/by/4.0/

This article has been accepted for publication in IEEE Open Journal of the Communications Society. This is the author's version which has not been fully edited and content may change prior to final publication. Citation information: DOI 10.1109/OJCOMS.2026.3741461

the PDL elements located between its injection point and the receiver. After inversion of the signal transfer function, this unequal propagation appears as a product of inverse PDL gains. With the ordering adopted throughout this paper, the inverse-SNR is therefore

$$\mathrm{SNR}_N^{-1} = \frac{p_{n,1}}{p_s} + \frac{1}{p_s}\sum_{i=1}^{N} p_{n,i+1}\prod_{k=1}^{i} A_k^{-1}. \tag{14}$$

Equation (14) makes the longitudinal dependence explicit: the i-th noise contribution is weighted by the cumulative inverse gain of only the first i PDL elements. Consequently, two links with the same total PDL and the same total ASE noise can exhibit different SNR statistics when the relative positions of the PDL elements and noise sources are changed, as observed in reversed-channel and distributed-link analyses [14], [16], [71].

For compactness, define the deterministic local noise-to-signal ratios

$$q_0 = \frac{p_{n,1}}{p_s}, \qquad q_i = \frac{p_{n,i+1}}{p_s}, \quad i = 1, \ldots, N. \tag{15}$$

Introducing the logarithmic increments and their partial sums,

$$Z_k = -\log(A_k), \qquad T_i = \sum_{k=1}^{i} Z_k, \tag{16}$$

transforms the product in (14) into an exponential. Hence,

$$\mathrm{SNR}_N^{-1} = q_0 + Y_N, \qquad Y_N = \sum_{i=1}^{N} q_i \exp(T_i). \tag{17}$$

Thus, the random part of the inverse-SNR is a weighted exponential functional of a random walk. The summands are strongly correlated because the partial sums T_i and T_j share the increments $Z_1, \ldots, Z_{\min(i,j)}$. This correlation is the central reason why replacing Y_N by a single elementary distribution is useful computationally but non-trivial statistically, especially in the outage-relevant tail.

The received SNR in dB is

$$\mathrm{SNR}_{N,\mathrm{dB}} = 10\log_{10}(\mathrm{SNR}_N). \tag{18}$$

For an operating threshold τ in dB, the probability of out-of-service is

$$P_{\mathrm{out}}(\tau) = \mathbb{P}\{\mathrm{SNR}_{N,\mathrm{dB}} \le \tau\} = \mathbb{P}\{Y_N \ge y_\tau\}, \tag{19}$$

where

$$y_\tau = 10^{-\tau/10} - q_0. \tag{20}$$

If $y_\tau \le 0$, then $P_{\mathrm{out}}(\tau) = 1$; otherwise, the outage probability is the survival function of the adopted approximation for Y_N evaluated at y_τ. Equivalently, for a target POOS ε, the required PDL margin is determined by the ε-quantile of $\mathrm{SNR}_{N,\mathrm{dB}}$. The remainder of the paper therefore focuses on efficient approximations of the distribution of Y_N, with particular attention to the accuracy of its right tail, which maps to the lower-SNR tail through (19).

V. DISTRIBUTIONAL APPROXIMATIONS

This section describes the approximations considered in this work. All of them model the random component $Y_N = \mathrm{SNR}_N^{-1} - q_0$. The deterministic shift q_0 is then reinserted when transforming to SNR or to SNR in dB.

For clarity, the presentation is organized according to the information used by each approximation. We first introduce the recursive moment framework, which is not itself a distributional approximation but a deterministic way to compute finite-length raw moments of Y_N. We then describe the approximations that use these recursively computed moments. Finally, we report the approximations that do not rely on the recursive moment model and instead use a Gaussian random-walk or log-delta representation.

A. Recursive Moment Framework

Define the backward random variable

$$R_i = \sum_{j=i}^{N} q_j \exp\left(\sum_{k=i}^{j} Z_k\right), \qquad R_{N+1} = 0. \tag{21}$$

Then

$$R_i = e^{Z_i}\left(q_i + R_{i+1}\right), \qquad Y_N = R_1. \tag{22}$$

Since Z_i is independent of R_{i+1}, the raw moments of R_i can be propagated backward along the link. Let

$$m_{r,i} = \mathbb{E}[R_i^r], \qquad r = 1, 2, 3, \tag{23}$$

and set $m_{0,i} = 1$. For $r = 1, 2, 3$,

$$m_{r,i} = \psi_i(r)\sum_{\ell=0}^{r}\binom{r}{\ell} q_i^{r-\ell} m_{\ell,i+1}, \tag{24}$$

with $m_{r,N+1} = 0$ for $r \ge 1$. In particular,

$$m_{1,i} = \psi_i(1)\left(q_i + m_{1,i+1}\right), \tag{25}$$

$$m_{2,i} = \psi_i(2)\left(q_i^2 + 2q_i m_{1,i+1} + m_{2,i+1}\right), \tag{26}$$

$$m_{3,i} = \psi_i(3)\left(q_i^3 + 3q_i^2 m_{1,i+1} + 3q_i m_{2,i+1} + m_{3,i+1}\right). \tag{27}$$

Thus $m_{r,1} = \mathbb{E}[Y_N^r]$. This recursion is exact for the finite-length model in (17); no Gaussian or lognormal assumption is made at this stage. It has $O(N)$ complexity for a fixed maximum moment order and only requires the local exponential moments $\psi_i(r) = \mathbb{E}[e^{rZ_i}]$.

The recursive framework is used by the gamma moment-matched approximation, the recursive moment-matched lognormal approximation, and the third-moment recursive log-skew-normal approximation. These methods differ only in the distribution chosen after the moments have been computed.

B. Gamma Moment-Matched Approximation

The gamma approximation models

$$Y_N \approx G, \qquad G \sim \mathrm{Gamma}(k, \theta), \tag{28}$$

where k is the shape parameter and θ is the scale parameter. The PDF of G is written as

$$f_G(x) = \frac{1}{\theta^k \Gamma(k)} x^{k-1} e^{-\frac{x}{\theta}}, \qquad x > 0, \tag{29}$$

This work is licensed under a Creative Commons Attribution 4.0 License. For more information, see https://creativecommons.org/licenses/by/4.0/

This article has been accepted for publication in IEEE Open Journal of the Communications Society. This is the author's version which has not been fully edited and content may change prior to final publication. Citation information: DOI 10.1109/OJCOMS.2026.3741461

where $\Gamma(k)$ is Euler's gamma function,

$$\Gamma(k) = \int_0^\infty t^{k-1} e^{-t}\, \mathrm{d}t. \tag{30}$$

Let

$$m_1 = \mathbb{E}[Y_N] = m_{1,1}, \qquad \sigma_Y^2 = \mathrm{Var}(Y_N) = m_{2,1} - m_{1,1}^2, \tag{31}$$

where $m_{1,1}$ and $m_{2,1}$ are obtained from the recursive moment framework in Section A. Moment matching gives

$$k = \frac{m_1^2}{\sigma_Y^2}, \qquad \theta = \frac{\sigma_Y^2}{m_1}. \tag{32}$$

The outage probability is

$$P_{\mathrm{out}}(\tau) \approx 1 - F_G(y_\tau), \qquad y_\tau > 0. \tag{33}$$

The gamma model is simple, positive, and numerically robust. However, it is not naturally matched to the multiplicative random-product structure of (17). Its exponential tail can be inaccurate when outage is driven by rare products with very small values of A_k. Therefore, it is best viewed as a baseline rather than as a tail-accurate model.

C. Recursive Moment-Matched Lognormal Approximation

The recursive moment-matched lognormal approximation uses the exact first two raw moments computed by (25)–(26) and approximates Y_N with a lognormal random variable. Matching

$$\mathbb{E}[Y_N] = m_{1,1}, \qquad \mathbb{E}[Y_N^2] = m_{2,1}, \tag{34}$$

gives

$$\sigma_L^2 = \log\left(\frac{m_{2,1}}{m_{1,1}^2}\right), \qquad \mu_L = \log(m_{1,1}) - \frac{1}{2}\sigma_L^2. \tag{35}$$

Then

$$Y_N \approx \mathrm{LN}(\mu_L, \sigma_L^2), \tag{36}$$

where the PDF of the lognormal distribution is

$$f_{\mathrm{LN}}(x) = \frac{1}{x\sqrt{2\pi\sigma_L^2}} \exp\left[-\frac{(\log(x) - \mu_L)^2}{2\sigma_L^2}\right], \qquad x > 0. \tag{37}$$

This approximation uses exact first and second moments of the finite-length recursion and has $O(N)$ complexity. It provides a finite-length scale match based on the exact first two raw moments. Its limitation is that it compresses the distribution into only two raw moments; it may miss skewness and may be inaccurate for very small outage probabilities.

D. Third-Moment Recursive Log-Skew-Normal Approximation

A higher-order recursive construction uses the first three exact raw moments obtained from (24). It assumes

$$Y_N \approx \exp(W), \qquad W \sim \mathrm{SN}(\xi, \omega, \alpha), \tag{38}$$

where the PDF of the skew-normal random variable W is

$$f_{\mathrm{SN}}(w) = \frac{2}{\omega}\,\phi\left(\frac{w-\xi}{\omega}\right)\Phi\left(\alpha\frac{w-\xi}{\omega}\right). \tag{39}$$

The moment-generating function of a skew-normal random variable is

$$\mathbb{E}[e^{tW}] = 2\exp\left(\xi t + \frac{1}{2}\omega^2 t^2\right)\Phi(\delta\omega t), \tag{40}$$

where $\delta = \alpha/\sqrt{1+\alpha^2}$, and $\phi(\cdot)$ and $\Phi(\cdot)$ are the standard normal PDF and CDF, respectively. The parameters ξ, ω, δ are found by matching

$$\log(m_{r,1}) = \log(2) + \xi r + \frac{1}{2}\omega^2 r^2 + \log(\Phi(\delta\omega r)), \tag{41}$$

for $r = 1, 2, 3$, and $\alpha = \delta/\sqrt{1-\delta^2}$.

This method is deterministic and retains exact finite-length information up to the third raw moment. It can be useful for tail-sensitive modeling because $m_{3,1}$ emphasizes large values of Y_N, which correspond to low SNR. However, this is also its main drawback: for large σ_{PDL}, the moments $\psi_i(2)$ and $\psi_i(3)$ can be dominated by rare events where A_i is close to zero. The resulting fit may overemphasize the far right tail of Y_N and distort the central density of the SNR in dB.

E. Correlated Fenton-Wilkinson Lognormal Approximation

The Fenton-Wilkinson method approximates a sum of lognormal variables by another lognormal distribution matched to the first two moments [21]. Unlike the recursive approximations above, this method does not use the finite-length moment recursion for Y_N. Instead, it approximates the random-walk vector $(T_1, \ldots, T_N)$ as multivariate Gaussian and then computes the moments of the resulting correlated lognormal sum. In the present setting, the variables $q_i \exp(T_i)$ are strongly correlated because the partial sums T_i share increments.

Approximate the random vector $(T_1, \ldots, T_N)$ as multivariate Gaussian with

$$M_i = \mathbb{E}[T_i] = \sum_{k=1}^{i} \mu_k, \qquad V_i = \mathrm{Var}(T_i) = \sum_{k=1}^{i} v_k, \tag{42}$$

$$C_{ij} = \mathrm{Cov}(T_i, T_j) = \sum_{k=1}^{\min(i,j)} v_k. \tag{43}$$

Then

$$\mathbb{E}[q_i e^{T_i}] = q_i \exp\left(M_i + \frac{1}{2}V_i\right), \tag{44}$$

while

$$\mathbb{E}[q_i e^{T_i} q_j e^{T_j}] = q_i q_j \times \exp\left(M_i + M_j + \frac{1}{2}(V_i + V_j) + C_{ij}\right). \tag{45}$$

Summing (45) over (i, j) gives the approximate first and second moments of Y_N, which are converted to lognormal parameters using (35).

This work is licensed under a Creative Commons Attribution 4.0 License. For more information, see https://creativecommons.org/licenses/by/4.0/

This article has been accepted for publication in IEEE Open Journal of the Communications Society. This is the author's version which has not been fully edited and content may change prior to final publication. Citation information: DOI 10.1109/OJCOMS.2026.3741461

The correlated Fenton-Wilkinson approximation accounts for the covariance induced by the random-walk structure and is usually more principled than treating the terms as independent lognormals. Its accuracy depends on how well the partial sums T_i are approximated as jointly Gaussian. In the generic case, the second-moment summation is $O(N^2)$, but with the prefix covariance structure it can often be reduced to $O(N)$ or near-linear complexity.

F. Delta-Cumulant Log-Skew-Normal Approximation

This approximation models Y_N as the exponential of a skew-normal random variable. Its parameters are obtained from the first three cumulants of a log-delta expansion of $\log(Y_N)$. It does not use the recursive raw moments of Y_N; instead, it propagates local cumulants of Z_i through a first-order log-sum-exp linearization. This name emphasizes both the modeling domain, namely the logarithm of the inverse-SNR random component, and the source of the fitted cumulants.

Define

$$D = \sum_{i=1}^{N} q_i e^{M_i}, \qquad \pi_i = \frac{q_i e^{M_i}}{D}, \tag{46}$$

where $M_i = \sum_{k=1}^{i} \mu_k$. Let

$$h_k = \sum_{i=k}^{N} \pi_i. \tag{47}$$

Writing $Z_k = \mu_k + \epsilon_k$, the first-order log-delta statistic is

$$W_\Delta = \log(D) + \sum_{k=1}^{N} h_k \epsilon_k \approx \log(Y_N). \tag{48}$$

The first-order cumulants of W_Δ are

$$\kappa_1 \approx \log(D), \tag{49}$$

$$\kappa_2 \approx \sum_{k=1}^{N} h_k^2 v_k, \tag{50}$$

$$\kappa_3 \approx \sum_{k=1}^{N} h_k^3 \kappa_{3,k}, \tag{51}$$

where $\kappa_{3,k}$ is the third cumulant of Z_k. A second-order bias correction to the mean is

$$\kappa_1 \approx \log(D) + \frac{1}{2}\sum_{k=1}^{N} v_k h_k (1 - h_k). \tag{52}$$

Additional second-order corrections may also be included in κ_2, but the essential skewness information is captured by (51).

Let

$$W \sim \mathrm{SN}(\xi, \omega, \alpha), \tag{53}$$

where ξ is location, $\omega > 0$ is scale, and α is shape [22]. Define

$$\delta = \frac{\alpha}{\sqrt{1+\alpha^2}}, \qquad b_\delta = \delta\sqrt{\frac{2}{\pi}}. \tag{54}$$

Then

$$\mathbb{E}[W] = \xi + \omega b_\delta, \tag{55}$$

$$\mathrm{Var}(W) = \omega^2(1 - b_\delta^2), \tag{56}$$

$$\gamma_1(W) = \frac{(4-\pi) b_\delta^3}{2(1-b_\delta^2)^{3/2}}. \tag{57}$$

Given κ_1, κ_2, and κ_3, one sets the target standardized skewness

$$\gamma_1^\star = \frac{\kappa_3}{\kappa_2^{3/2}}, \tag{58}$$

solves numerically for δ, and then obtains

$$\omega = \sqrt{\frac{\kappa_2}{1 - b_\delta^2}}, \qquad \xi = \kappa_1 - \omega b_\delta. \tag{59}$$

The model for the random inverse-SNR component is

$$Y_N \approx \exp(W), \qquad W \sim \mathrm{SN}(\xi, \omega, \alpha). \tag{60}$$

This approximation is deterministic, typically $O(N)$, and captures a leading asymmetry of $\log Y_N$ that a normal or lognormal approximation misses. Its main weakness is that it is still a local delta approximation. It may be inaccurate when σ^2_{PDL} is large, when the log-sum-exp nonlinearity is strong, or when the target outage lies far in the tail.

VI. DIGITAL-TWIN DISAGGREGATION AND OUTAGE EVALUATION

The approximations in the previous section have different levels of compatibility with a network digital twin. In this context, an approximation is called *disaggregable* if each optical element can contribute a small set of local quantities, and if the digital twin can combine these quantities along the selected lightpath without simulating the full random link.

For the i-th PDL element, the local quantities are the cumulants or exponential moments of

$$Z_i = -\log(A_i). \tag{61}$$

Typical examples are

$$\mu_i = \mathbb{E}[Z_i], \quad v_i = \mathrm{Var}(Z_i), \quad \kappa_{3,i} = \mathrm{cum}_3(Z_i), \tag{62}$$

and

$$b_{r,i} = \mathbb{E}[e^{rZ_i}] = \mathbb{E}[A_i^{-r}], \qquad r = 1, 2, 3. \tag{63}$$

For Maxwell-distributed PDL, these quantities can be obtained from one-dimensional integration over the local PDL distribution. Conditionally on γ_i, for $r \neq 1$,

$$\mathbb{E}[A_i^{-r} \mid \gamma_i] = \frac{(1+\gamma_i)^{1-r} - (1-\gamma_i)^{1-r}}{2\gamma_i(1-r)}, \tag{64}$$

while

$$\mathbb{E}[A_i^{-1} \mid \gamma_i] = \frac{\mathrm{artanh}(\gamma_i)}{\gamma_i}. \tag{65}$$

Thus, each device can expose a compact set of moment descriptors rather than a full probability law.

This work is licensed under a Creative Commons Attribution 4.0 License. For more information, see https://creativecommons.org/licenses/by/4.0/

This article has been accepted for publication in IEEE Open Journal of the Communications Society. This is the author's version which has not been fully edited and content may change prior to final publication. Citation information: DOI 10.1109/OJCOMS.2026.3741461

A. Disaggregability of the Approximation Families

The gamma approximation, the recursive moment-matched lognormal approximation, and the third-moment recursive log-skew-normal approximation are fully disaggregable through moment recursion. Each device contributes only the local exponential moments of its inverse gain, and the digital twin combines these descriptors along the selected lightpath.

They rely on the backward recursion (22) and on the local exponential moments $b_{r,i}$ in (63). For the first three raw moments,

$$m_{r,i} = b_{r,i} \sum_{\ell=0}^{r} \binom{r}{\ell} q_i^{r-\ell} m_{\ell,i+1}, \qquad r = 1,2,3, \tag{66}$$

with $m_{0,i} = 1$ and $m_{r,N+1} = 0$ for $r \geq 1$. Therefore, the first, second, and third moments of Y_N can be computed with $O(N)$ operations and a constant-size state. The gamma and recursive lognormal approximations use $m_{1,1}$ and $m_{2,1}$, whereas the third-moment recursive log-skew-normal approximation also uses $m_{3,1}$.

The correlated Fenton-Wilkinson approximation is disaggregable with a slightly more global state. The digital twin accumulates

$$M_i = \sum_{k=1}^{i} \mu_k, \qquad V_i = \sum_{k=1}^{i} v_k, \tag{67}$$

and then evaluates the first two moments of the correlated lognormal sum. The covariance structure

$$\mathrm{Cov}(T_i, T_j) = V_{\min(i,j)} \tag{68}$$

is inherited from the random walk. In a direct implementation, the second moment requires a double sum, but the prefix structure can be exploited to obtain a linear or near-linear implementation for many practical coefficient profiles.

The delta-cumulant log-skew-normal approximation is partially disaggregable. It uses local cumulants, but it also requires the log-delta weights

$$h_k = \frac{\sum_{i=k}^{N} q_i e^{M_i}}{\sum_{i=1}^{N} q_i e^{M_i}}. \tag{69}$$

These weights are tail sums over the remaining lightpath. Hence, a practical implementation uses two passes: a forward pass computes M_i and the normalizing denominator, and a backward pass computes the tail sums in (69). Once the weights are available, the cumulants add element by element.

B. Forward Moment Accumulation Along a Lightpath

Although (66) is compact, a digital twin may naturally process the lightpath in the forward direction. This is also possible by maintaining moments of the inverse product and of the accumulated inverse-SNR contribution.

Let

$$P_i = \prod_{k=1}^{i} A_k^{-1}, \qquad Y_i = \sum_{j=1}^{i} q_j P_j, \tag{70}$$

with $P_0 = 1$ and $Y_0 = 0$. When element i is appended,

$$P_i = P_{i-1} B_i, \qquad Y_i = Y_{i-1} + q_i P_i, \qquad B_i = A_i^{-1}. \tag{71}$$

For moments up to order three, define the state variables

$$\begin{aligned} p_r &= \mathbb{E}[P^r], \qquad r = 1,2,3, \\ s_r &= \mathbb{E}[Y^r], \qquad r = 1,2,3, \\ c_{11} &= \mathbb{E}[YP], \quad c_{12} = \mathbb{E}[YP^2], \quad c_{21} = \mathbb{E}[Y^2 P]. \end{aligned} \tag{72}$$

With $b_r = \mathbb{E}[B_i^r]$, the product moments update as

$$p_r' = b_r p_r, \qquad r = 1,2,3. \tag{73}$$

The accumulated moments update as

$$s_1' = s_1 + q_i p_1', \tag{74}$$

$$s_2' = s_2 + 2 q_i b_1 c_{11} + q_i^2 p_2', \tag{75}$$

$$s_3' = s_3 + 3 q_i b_1 c_{21} + 3 q_i^2 b_2 c_{12} + q_i^3 p_3'. \tag{76}$$

The auxiliary cross-moments update according to

$$c_{11}' = b_1 c_{11} + q_i p_2', \tag{77}$$

$$c_{12}' = b_2 c_{12} + q_i p_3', \tag{78}$$

$$c_{21}' = b_1 c_{21} + 2 q_i b_2 c_{12} + q_i^2 p_3'. \tag{79}$$

The initialization is

$$\begin{aligned} p_1 = p_2 = p_3 = 1, \\ s_1 = s_2 = s_3 = 0, \\ c_{11} = c_{12} = c_{21} = 0. \end{aligned} \tag{80}$$

After the last device, s_1, s_2, and s_3 are the first three raw moments of Y_N. This forward form is convenient when the digital twin builds or updates the lightpath device by device.

C. Multi-Vendor and Multi-Operator Parameter Exchange

A practical multi-vendor lightpath is generally inhomogeneous. The per-element standard deviation may depend on the vendor, device family, WSS port, programmed attenuation, spectral region, and administrative domain. Thus, the i-th element can be characterized by

$$\mathrm{Var}(X_i) = \sigma_{\mathrm{PDL},i}^2, \qquad b_{r,i} = \mathbb{E}[A_i^{-r}], \quad r = 1,2,3, \tag{81}$$

with $b_{r,i}$ evaluated from its own PDL prior. None of the moment recursions requires a common σ_{PDL}: core, metro, access, or vendor-specific portions can use different values without changing the end-to-end algorithm.

From an operator perspective, sharing only the number of devices, one aggregate σ_{PDL}, total ASE power, and total insertion loss is generally insufficient. Such scalars discard the longitudinal ordering between the noise injections and the PDL elements, which is precisely the information that determines the coefficients in (17). At the opposite extreme, requiring every domain to disclose its complete node topology, WSS settings, amplifier inventory, and per-device PDL law would be operationally heavy and may conflict with commercial confidentiality.

The forward recursion above enables a privacy-preserving compromise. For the third-order model, define the constant-size state

$$\mathbf{x} = \big(p_1, p_2, p_3, s_1, s_2, s_3, c_{11}, c_{12}, c_{21}\big)^{\mathsf{T}}. \tag{82}$$

This work is licensed under a Creative Commons Attribution 4.0 License. For more information, see https://creativecommons.org/licenses/by/4.0/

This article has been accepted for publication in IEEE Open Journal of the Communications Society. This is the author's version which has not been fully edited and content may change prior to final publication. Citation information: DOI 10.1109/OJCOMS.2026.3741461

An operator can receive $\mathbf{x}_{\text{in}}$, apply the internal sequence of q_i and $b_{r,i}$ values without revealing it, and return only $\mathbf{x}_{\text{out}}$. Hence, only nine real-valued state entries are exchanged per domain for the third-moment approximation; the two-moment gamma and lognormal models require only the reduced five-entry state $(p_1, p_2, s_1, s_2, c_{11})$. For repeated queries, the same operation may equivalently be exposed as a constant-size linear transition

$$\mathbf{x}_{\text{out}} = \mathsf{M}_d \mathbf{x}_{\text{in}}, \tag{83}$$

where M_d summarizes domain d while preserving the effect of its internal longitudinal ordering.

A minimal inter-operator contract should additionally declare the common single-polarization power normalization, the signal power or ROP at the domain boundaries, the deterministic endpoint inverse-SNR term (or, equivalently, the transceiver SNR), and the validity metadata of the descriptor, including carrier frequency, symbol rate, roll-off or occupied bandwidth, operating configuration, timestamp, and uncertainty or confidence level. This information is much lighter than the full network specification, yet it is sufficient to compose an outage distribution consistently. When only coarse descriptors such as $(N_d, \sigma_{\text{PDL},d})$ and total ASE are available, the resulting loss of longitudinal information should instead be represented by an additional modeling uncertainty or engineering margin.

D. Analytical Outage Evaluation

For all approximations, outage is evaluated through the survival function of Y_N. For a threshold τ in dB, define

$$y_\tau = 10^{-\tau/10} - q_0. \tag{84}$$

Then

$$P_{\text{out}}(\tau) = \begin{cases} \mathbb{P}\{Y_N \geq y_\tau\}, & y_\tau > 0, \\ 1, & y_\tau \leq 0. \end{cases} \tag{85}$$

The case $y_\tau \leq 0$ occurs when the threshold is above the maximum SNR allowed by the deterministic shift q_0, namely $\text{SNR}_{\max} = 1/q_0$.

For any lognormal approximation $Y_N \sim \text{LN}(\mu_L, \sigma_L^2)$,

$$P_{\text{out}}(\tau) \approx \bar{\Phi}\left(\frac{\log(y_\tau) - \mu_L}{\sigma_L}\right), \qquad y_\tau > 0, \tag{86}$$

where $\bar{\Phi}(\cdot) = 1 - \Phi(\cdot)$. This formula applies to the recursive moment-matched lognormal and correlated Fenton-Wilkinson lognormal models.

For the gamma approximation $Y_N \sim \text{Gamma}(k, \theta)$,

$$P_{\text{out}}(\tau) \approx Q\left(k, \frac{y_\tau}{\theta}\right), \qquad y_\tau > 0, \tag{87}$$

where $Q(k, x) = \Gamma(k, x)/\Gamma(k)$ is the regularized upper incomplete gamma function.

For log-skew-normal models, write

$$Y_N \approx \exp(W), \qquad W \sim \text{SN}(\xi, \omega, \alpha). \tag{88}$$

Then

$$P_{\text{out}}(\tau) \approx 1 - F_{\text{SN}}\left(\frac{\log(y_\tau) - \xi}{\omega}; \alpha\right), \qquad y_\tau > 0. \tag{89}$$

The skew-normal CDF can be evaluated using standard numerical libraries or through Owen's T function,

$$F_{\text{SN}}(z; \alpha) = \Phi(z) - 2T(z, \alpha). \tag{90}$$

This formula applies both to the delta-cumulant log-skew-normal approximation and to the third-moment recursive log-skew-normal approximation.

Table 2 summarizes the digital-twin implementation viewpoint. The most suitable method depends on whether the objective is central distributional accuracy, tail probability, or a very low-complexity online update.

E. Comparison of the Approximations and Practical Guidelines

Table 3 summarizes the methods. The complexity is stated per operating point, excluding the precomputation of the PDL moments.

For outage estimation, the most relevant distinction is whether the approximation accurately models the right tail of Y_N. Central metrics, such as a Kolmogorov-Smirnov distance over the entire CDF, can be dominated by the center of the dB-domain distribution and may not directly indicate outage accuracy. Conversely, moment-based methods that emphasize high raw moments may improve tail behavior but degrade the central density. A digital-twin implementation should therefore report both global distributional metrics and tail-specific metrics such as the error in $\log_{10} P_{\text{out}}(\tau)$ over a target outage range.

For low σ_{PDL} and moderate N, the SNR distribution can be narrow. In that regime, small location errors in $\log(Y_N)$ may produce large Kolmogorov-Smirnov distances, even if outage predictions over a practical threshold range are acceptable. For moderate σ_{PDL}, recursive moment-matched lognormal and correlated Fenton-Wilkinson approximations usually provide better finite-length scale matching. The two log-skew-normal methods are preferable when the goal is to retain log-domain asymmetry or third-moment information rather than only match the first two moments.

For large σ_{PDL}, skewness and rare events become important. The delta-cumulant log-skew-normal approximation provides a controlled way to introduce asymmetry on the logarithmic scale. The third-moment recursive log-skew-normal method is more tail-sensitive, but it should be interpreted carefully because $\mathbb{E}[A^{-3}]$ can be large when A has appreciable probability mass near zero.

VII. MONTE CARLO VALIDATION

In the validation simulations reported in this section, we consider links with uniformly distributed noise loading along the line. Consistently with Sections I and D, all signal- and noise-power values quoted in this section refer to one of the two recovered polarization axes, i.e., to a single polarization tributary, rather than to the total dual-polarization power. Specifically, unless otherwise stated, all noise contributions are assigned the same power, namely $p_{n,i} = -25$ dBm

This work is licensed under a Creative Commons Attribution 4.0 License. For more information, see https://creativecommons.org/licenses/by/4.0/

This article has been accepted for publication in IEEE Open Journal of the Communications Society. This is the author's version which has not been fully edited and content may change prior to final publication. Citation information: DOI 10.1109/OJCOMS.2026.3741461

TABLE 2. Digital-twin implementation and outage evaluation.

Approximation	Disaggregation state	Outage expression
Gamma	m_1, m_2 from moment recursion	Gamma survival (87)
Recursive lognormal	m_1, m_2 from backward or forward recursion	Lognormal survival (86)
Third-moment recursive log-skew-normal	m_1, m_2, m_3 from moment recursion	Skew-normal survival (89)
Fenton-Wilkinson	Prefix means/variances and correlated second moment of the lognormal sum	Lognormal survival (86)
Delta-cumulant log-skew-normal	Two-pass weights h_i and local cumulants of Z_i	Skew-normal survival (89)

TABLE 3. Summary of inverse-SNR approximations for $Y_N = \mathrm{SNR}_N^{-1} - q_0$.

Approximation	Principle and cost	Strengths / limitations
Gamma	Match $\mathbb{E}[Y_N]$ and $\mathrm{Var}(Y_N)$ to $\mathrm{Gamma}(k,\theta)$; $O(N)$ with recursive moments.	Positive and simple, but tail shape is not naturally matched to products.
Recursive lognormal	Exact first two moments from the backward recursion; $O(N)$.	Good scale matching, but only two raw moments and limited tail control.
Third-moment recursive log-skew-normal	Recursive $\mathbb{E}[Y_N]$, $\mathbb{E}[Y_N^2]$, and $\mathbb{E}[Y_N^3]$, then $Y_N \approx \exp(W)$.	Tail-sensitive, but high raw moments may be dominated by rare $A \approx 0$ events.
Correlated Fenton-Wilkinson	Gaussian approximation of (T_i), correlated lognormal sum moment matching.	Accounts for random-walk covariance, but depends on Gaussian partial sums.
Delta-cumulant log-skew-normal	$Y_N \approx \exp(W)$, with W skew-normal and fitted from log-delta cumulants; $O(N)$.	Captures log-domain skewness, but remains local.

for $i = 1, \ldots, N+1$, while the signal power is set to $p_s = 0$ dBm. These values keep the resulting SNR range and noise-to-signal ratios in a regime representative of realistic optical-link conditions. The validation grid then increases both the number of PDL elements N and the per-element PDL standard deviation σ_{PDL}, testing the approximations from short, weak-PDL links to longer links with stronger accumulated fluctuations. For this uniformly distributed noise case, changing every noise power by the same amount does not materially change the reported shape-based metrics. Indeed, if $p_{n,i} = p_n$ for all i, then all $q_i = p_n/p_s$ are multiplied by the same factor and the inverse-SNR becomes a common scale factor times a random term that depends only on the PDL variables. In the dB domain, this common scaling produces a rigid translation of the SNR distribution. Therefore, the global shape metrics and the quantile-based outage errors evaluated at empirical outage levels are essentially invariant to a uniform change of p_n. Section VIII deliberately removes this symmetry by considering realistic, strongly non-uniform noise and PDL profiles.

The Monte Carlo simulator is the one developed in [18] and subsequently used in [15], [72]. No external dataset is used in this validation: the empirical SNR distributions are generated from the stochastic link model and the parameters stated below. Each PDL-induced SNR distribution was obtained from 10^9 realizations with random polarization scrambling between consecutive PDL elements, according to the hinge model [19], and with an independent Maxwell-distributed PDL magnitude for each element as defined in Section B. The standard deviation σ_{PDL} ranges from 0.1 to 1.5 dB in 0.05-dB steps, and the number of elements is $N \in \{2, 10, 40\}$, spanning short, intermediate, and long cascades. Each empirical distribution is represented by a 120-bin histogram. The analytical parameters are obtained from the assumed PDL prior and the deterministic noise coefficients; they are not fitted to the Monte Carlo histograms. For the uniformly distributed ASE model considered in this section, the campaign evaluates every combination in the stated $(N, \sigma_{\mathrm{PDL}})$ grid. The following subsection defines both global distributional metrics and tail-oriented metrics selected to assess outage prediction and ONDT margin accuracy.

A. Distributional and Tail-Oriented Accuracy Metrics

The Monte Carlo validation compares each analytical approximation against an empirical reference distribution of the received SNR in dB. Let $S_1, \ldots, S_M$ denote the Monte Carlo samples of $\mathrm{SNR}_{N,\mathrm{dB}}$, and let

$$\widehat{F}_M(s) = \frac{1}{M} \sum_{m=1}^{M} \mathbf{1}\{S_m \le s\}, \tag{91}$$

be the empirical CDF. For a given approximation a, we denote by $F_a(s)$ the corresponding CDF of $\mathrm{SNR}_{N,\mathrm{dB}}$, obtained from the analytical survival function of Y_N as described in Section D. Since outage estimation is a tail problem, we use both global distributional metrics and metrics explicitly targeted to the left tail of $\mathrm{SNR}_{N,\mathrm{dB}}$.

The first global metric is the Kolmogorov-Smirnov distance

$$D_{\mathrm{KS}}^{(a)} = \sup_s \left| \widehat{F}_M(s) - F_a(s) \right|. \tag{92}$$

This metric is non-parametric and measures the largest vertical discrepancy between the empirical and analytical CDFs, following the standard Kolmogorov-Smirnov goodness-of-fit statistic [74], [75], [76]. It is useful to detect global CDF

This work is licensed under a Creative Commons Attribution 4.0 License. For more information, see https://creativecommons.org/licenses/by/4.0/

This article has been accepted for publication in IEEE Open Journal of the Communications Society. This is the author's version which has not been fully edited and content may change prior to final publication. Citation information: DOI 10.1109/OJCOMS.2026.3741461

mismatch, but it may be dominated by the central part of the distribution, especially when the SNR distribution is narrow.

The second global metric is an RMSE between probability masses on a common histogram grid. Let $\{\mathcal{B}_b\}_{b=1}^{B}$ be bins on the SNR-dB axis, and define

$$\widehat{p}_b = \frac{1}{M}\sum_{m=1}^{M} \mathbf{1}\{S_m \in \mathcal{B}_b\}, \qquad p_{a,b} = \int_{\mathcal{B}_b} \mathrm{d}F_a(s). \quad (93)$$

The mass RMSE is

$$\mathrm{RMSE}^{(a)}_{\mathrm{mass}} = \sqrt{\frac{1}{B}\sum_{b=1}^{B} (\widehat{p}_b - p_{a,b})^2}. \quad (94)$$

This metric summarizes the average mismatch between empirical and analytical bin probabilities. It is less sensitive than the Kolmogorov-Smirnov distance to a single worst point of the CDF, and RMSE-type criteria are widely used for model-evaluation purposes [77].

The third global metric is the discrete Kullback-Leibler divergence from the empirical distribution to the model distribution,

$$D_{\mathrm{KL}}\left(\widehat{p} \,\|\, p_a\right) = \sum_{b:\widehat{p}_b>0} \widehat{p}_b \log\left(\frac{\widehat{p}_b}{p_{a,b}}\right), \quad (95)$$

where small positive floors are used in the numerical implementation to avoid divisions by zero. The Kullback-Leibler divergence measures an information-theoretic discrepancy between probability laws [78]. In this work it is used only as a finite-bin diagnostic, since its value depends on the selected binning and can be sensitive to very small model probabilities.

The previous metrics evaluate the distribution globally. However, the optical-network digital-twin use case is driven by probabilities of out-of-service in the range

$$\mathcal{P}_{\mathrm{OOS}} = \{10^{-6}, 10^{-5}, 10^{-4}\}, \quad (96)$$

or, in less stringent diagnostic runs, with the additional level 10^{-3}. These probabilities correspond to the extreme left tail of the SNR distribution and are directly related to outage-based margin design, as in PDL-aware outage analyses for optical links [15], [66]. Therefore, we also use two tail-oriented metrics.

For each target probability $p \in \mathcal{P}_{\mathrm{OOS}}$, let

$$\widehat{\tau}_p = \widehat{F}_M^{-1}(p), \quad (97)$$

be the empirical left-tail SNR-dB quantile. The first outage-oriented metric evaluates whether the analytical model assigns the correct outage probability at the Monte Carlo outage thresholds:

$$\mathrm{RMSE}^{(a)}_{\log_{10}(P_{\mathrm{out}})} = \sqrt{\frac{1}{|\mathcal{P}_{\mathrm{OOS}}|}\sum_{p\in\mathcal{P}_{\mathrm{OOS}}} [\log_{10} F_a(\widehat{\tau}_p) - \log_{10} p]^2}. \quad (98)$$

This metric measures the outage error in orders of magnitude. For example, an error of 0.3 approximately corresponds to a factor-of-two error in outage probability, whereas an error of 1 corresponds to one decade.

The second outage-oriented metric is a quantile RMSE in dB. Let

$$\tau_{a,p} = F_a^{-1}(p), \quad (99)$$

be the analytical SNR-dB quantile associated with the same target outage probability. We define

$$\mathrm{RMSE}^{(a)}_{Q,\mathrm{dB}} = \sqrt{\frac{1}{|\mathcal{P}_{\mathrm{OOS}}|}\sum_{p\in\mathcal{P}_{\mathrm{OOS}}} (\tau_{a,p} - \widehat{\tau}_p)^2}. \quad (100)$$

This metric is directly interpretable as an SNR-margin error in dB and is therefore particularly relevant for QoT-margin selection. Quantile-based criteria are standard tools for describing distribution tails and risk levels [79], [80].

A practical limitation is that Monte Carlo validation of very small probabilities requires a sufficiently large number of samples. If Mp is close to or below one, the empirical quantile $\widehat{\tau}_p$ and the empirical outage estimate are poorly resolved. In the numerical implementation, a probability floor of order $1/M$ is therefore used when evaluating logarithms, and the results at 10^{-6} should be interpreted cautiously unless the Monte Carlo sample size is much larger than 10^6 or variance-reduction techniques are introduced.

For the present sample size $M = 10^9$, the expected numbers of samples below the 10^{-6}, 10^{-5}, and 10^{-4} quantiles are 10^3, 10^4, and 10^5, respectively. Under binomial sampling, the corresponding relative standard errors of the empirical outage probabilities are approximately 3.16%, 1.00%, and 0.316%. These values provide the Monte Carlo resolution against which the reported tail errors should be interpreted.

B. Results

Figures 3 and 4 report the validation results as a function of the per-element Maxwell PDL standard deviation σ_{PDL}. The three columns correspond to $N = 2$, 10, and 40 PDL elements, respectively, so that the grid spans short cascades, representative intermediate links, and unusually long sequences of PDL-bearing elements. Experimental WSS characterizations covering different ports, frequencies, and programmed attenuation settings indicate substantially smaller device-level variability [16], [17]; in particular, the complete measurement set reported in [16] has an overall σ_{PDL} of 0.14 dB. In the following discussion, $\sigma_{\mathrm{PDL}} = 1$ dB is therefore used as a practical partition rather than as a limiting case or a boundary of the validation domain. Values below this point cover the conditions more readily encountered in optical networks, while the interval from 1 to 1.5 dB probes progressively stronger per-element PDL variability that is increasingly unlikely to be encountered in practical deployments. The $N = 40$ cases further amplify the severity of both regions by accumulating the impairment over a particularly large number of elements.

Figure 3 first compares the approximations according to the global CDF and probability-mass metrics. The gamma approximation is consistently the least accurate, confirming that an exponential-tail distribution is not well matched to

This work is licensed under a Creative Commons Attribution 4.0 License. For more information, see https://creativecommons.org/licenses/by/4.0/

This article has been accepted for publication in IEEE Open Journal of the Communications Society. This is the author's version which has not been fully edited and content may change prior to final publication. Citation information: DOI 10.1109/OJCOMS.2026.3741461

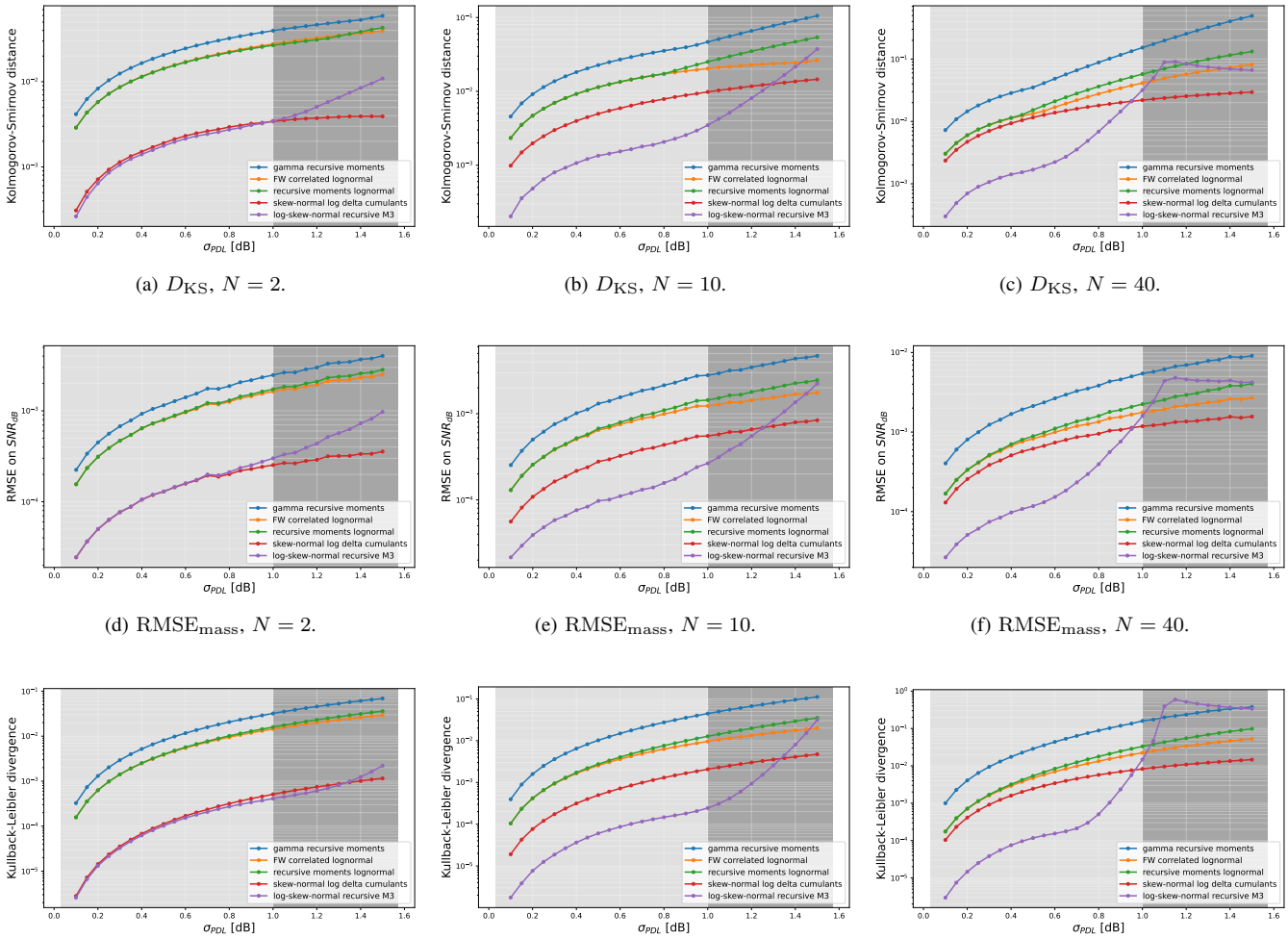

(a) D_{KS}, $N = 2$. (b) D_{KS}, $N = 10$. (c) D_{KS}, $N = 40$.

(d) $\mathrm{RMSE}_{\mathrm{mass}}$, $N = 2$. (e) $\mathrm{RMSE}_{\mathrm{mass}}$, $N = 10$. (f) $\mathrm{RMSE}_{\mathrm{mass}}$, $N = 40$.

(g) D_{KL}, $N = 2$. (h) D_{KL}, $N = 10$. (i) D_{KL}, $N = 40$.

FIGURE 3. Global distributional metrics versus the per-element Maxwell PDL standard deviation σ_{PDL} for $N = 2$, 10, and 40. Lower values indicate closer agreement with the Monte Carlo reference. The portion with darker background represents links with extreme PDL that are less likely to be found in real applications.

the multiplicative structure of the inverse-SNR. The correlated Fenton–Wilkinson and recursive lognormal models form an intermediate group: they reproduce the overall scale of the distribution reasonably well, but their two-moment descriptions cannot fully capture its asymmetry. Both log-skew-normal models provide a substantially closer global fit over most of the grid.

No single approximation is uniformly optimal over the complete 0.1–1.5 dB interval. In particular, the third-moment recursive log-skew-normal model is not the absolute best when the largest values of σ_{PDL} are included. Its global errors increase rapidly beyond approximately 1 dB, most visibly for $N = 40$, where the third raw moment is increasingly dominated by rare realizations with very small multiplicative gains. This behavior is consistent with the sensitivity to $\mathbb{E}[A^{-3}]$ discussed in Section V. In that high-variance region, the delta-cumulant log-skew-normal approximation generally provides the lowest and most regular KS, mass-RMSE, and KL curves.

The ranking changes in the range more readily encountered in optical networks. For $\sigma_{\mathrm{PDL}} < 1$ dB, the third-moment recursive log-skew-normal approximation is generally the best global model, or numerically comparable to the best one, for all three cascade lengths. Its advantage is especially clear for $N = 10$ and $N = 40$, where it retains the finite-length information contained in the exact first three moments instead of relying on Gaussian partial sums or on a local log-delta linearization. The absolute metric values are also encouraging, rather than merely favorable in a relative comparison. For the two skew-normal approximations, the KS distance is typically between 10^{-4} and a few 10^{-2}, the mass RMSE remains approximately between 10^{-5} and a few 10^{-3}, and the binned KL divergence is generally between 10^{-6} and a few 10^{-2} throughout the sub-1 dB region. Even around $\sigma_{\mathrm{PDL}} = 1$ dB with $N = 40$, the best models retain a

This work is licensed under a Creative Commons Attribution 4.0 License. For more information, see https://creativecommons.org/licenses/by/4.0/

This article has been accepted for publication in IEEE Open Journal of the Communications Society. This is the author's version which has not been fully edited and content may change prior to final publication. Citation information: DOI 10.1109/OJCOMS.2026.3741461

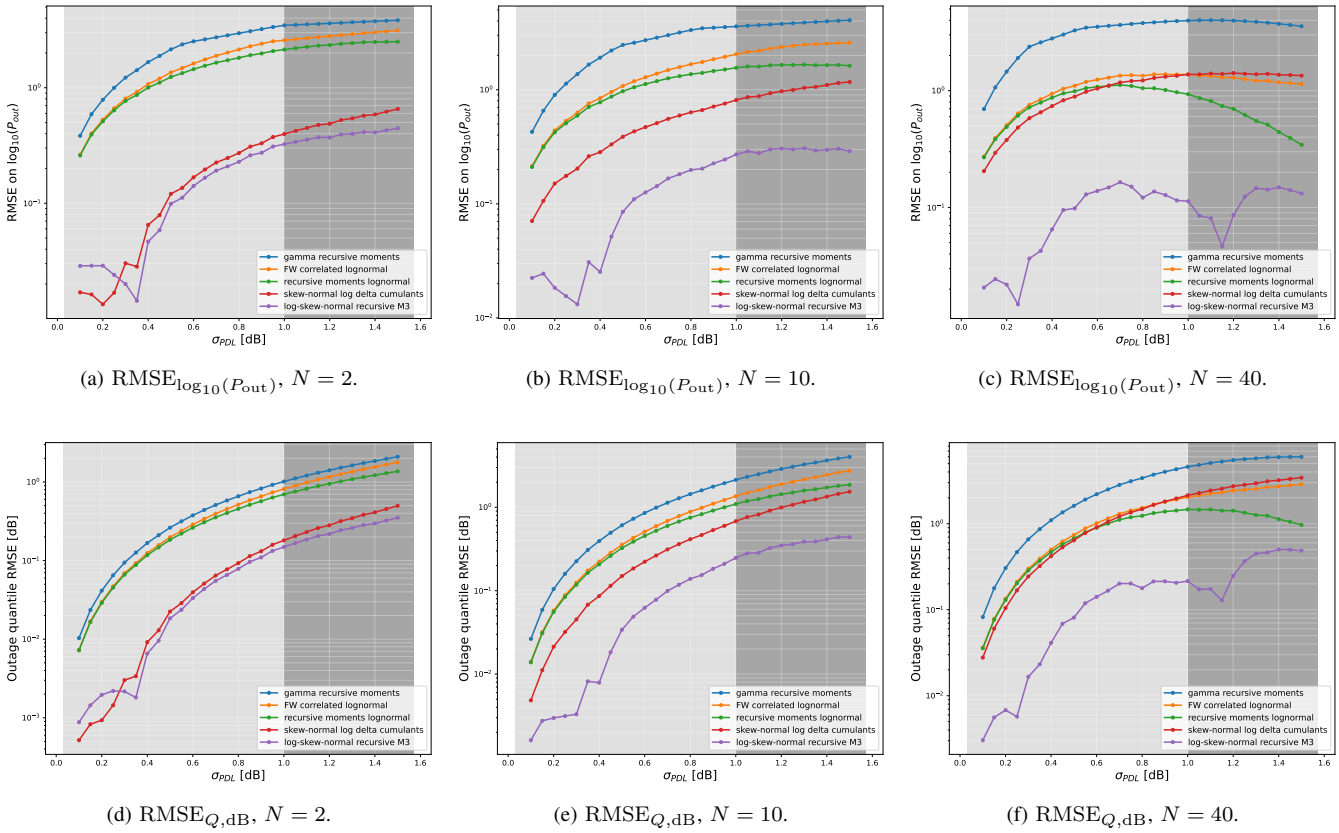

(a) $\mathrm{RMSE}_{\log_{10}(P_{\mathrm{out}})}$, $N = 2$. (b) $\mathrm{RMSE}_{\log_{10}(P_{\mathrm{out}})}$, $N = 10$. (c) $\mathrm{RMSE}_{\log_{10}(P_{\mathrm{out}})}$, $N = 40$.

(d) $\mathrm{RMSE}_{Q,\mathrm{dB}}$, $N = 2$. (e) $\mathrm{RMSE}_{Q,\mathrm{dB}}$, $N = 10$. (f) $\mathrm{RMSE}_{Q,\mathrm{dB}}$, $N = 40$.

FIGURE 4. Tail-oriented outage metrics versus the per-element Maxwell PDL standard deviation σ_{PDL} for $N = 2$, 10, and 40. The upper row measures the error in outage probability in decades, whereas the lower row measures the corresponding SNR-quantile error in decibels. The portion with darker background represents links with extreme PDL that are less likely to be found in real applications.

KS discrepancy of only a few percent and a mass RMSE of the order of 10^{-3}. Since this point combines a long cascade with a per-element variability located at the transition toward the high-PDL portion of the sweep, these values indicate that a compact analytical distribution can reproduce the Monte Carlo law with useful fidelity.

The global metrics, however, are not sufficient to select an approximation for an ONDT, because a small central-distribution error does not guarantee an accurate lower-SNR tail. Figure 4 therefore provides the decisive comparison. The gamma, Fenton–Wilkinson, and recursive lognormal approximations can exhibit errors approaching or exceeding one decade in P_{out} and several tenths of a decibel in the outage quantile as N or σ_{PDL} increases. The delta-cumulant log-skew-normal model improves substantially on these two-moment approximations, but its tail error still grows for long cascades and large per-element variability.

The third-moment recursive log-skew-normal approximation gives the most accurate outage prediction over almost the entire validation grid, apart from a few isolated very-low-PDL points for the shortest cascade. In the more commonly encountered range $\sigma_{\mathrm{PDL}} < 1$ dB, its logarithmic outage RMSE is generally limited to a few tenths of a decade, corresponding to a probability error well below one order of magnitude, while its outage-quantile RMSE is typically about 0.2 dB or less. The result remains strong at the transition toward the high-PDL regime: for $N = 40$ and $\sigma_{\mathrm{PDL}} \simeq 1$ dB, the model maintains an outage-probability error of roughly one tenth of a decade and an outage-margin error of roughly 0.2 dB, whereas the competing approximations are near or above one decade and approximately 1 dB, respectively. Thus, matching the third raw moment may slightly sacrifice central accuracy in the less likely high-PDL region above 1 dB, but it provides precisely the tail sensitivity required for POOS-based margin assessment.

Overall, the simulations support two complementary conclusions. First, the proposed low-complexity distributional approach is viable: several approximations reproduce the global SNR statistics accurately even under strongly adverse conditions. Second, for ONDT applications the third-moment recursive log-skew-normal model is the preferred approximation, because it combines disaggregable $O(N)$ moment accumulation with the best accuracy in the outage-relevant tail and with excellent global performance in the more commonly encountered sub-1 dB regime. Its behavior beyond that regime also provides a useful warning that very high raw moments should not be used without checking whether

This work is licensed under a Creative Commons Attribution 4.0 License. For more information, see https://creativecommons.org/licenses/by/4.0/

This article has been accepted for publication in IEEE Open Journal of the Communications Society. This is the author's version which has not been fully edited and content may change prior to final publication. Citation information: DOI 10.1109/OJCOMS.2026.3741461

the assumed device-level PDL prior assigns excessive weight to near-singular gains.

VIII. APPLICATIONS

The Monte Carlo campaign in Section VII intentionally used a uniform noise loading to isolate the statistical accuracy of the approximations over a broad range of N and σ_{PDL}. This section complements that controlled experiment with network configurations whose losses, amplifier noise figures, transceiver settings, and longitudinal placement of ASE and PDL are representative of operational optical links. The transmitter is common to all cases: the carrier frequency is $f_0 = 193.1$ THz, the symbol rate is $R_s = 61.3$ GBaud, the roll-off factor is 0.15, and the launched power is 3 dBm in total over the two polarizations. Under equal polarization loading, this corresponds to approximately 0 dBm on each polarization axis. The PDL standard deviation for each WSS element was set to $\sigma_{\mathrm{PDL}} = 0.5$ dB, thereby representing strong PDL effects.

The core section consists of five 100-km spans, for a total length of 500 km. Each span introduces 20 dB attenuation, each traversed core WSS has 10 dB insertion loss, the pre-amplifier noise figure (NF) is 5 dB, and the booster-amplifier NF is 6.5 dB. In the metro section, each 40-km span introduces 8 dB attenuation, the WSS insertion loss is 5 dB, the pre-amplifier NF is 8.5 dB, and the booster-amplifier NF is 6.5 dB. These are deliberately realistic component values commonly encountered in core and metro design, rather than parameters tuned to produce a convenient analytical distribution.

The application links are also substantially more demanding than the uniform-loading validation cases. ASE is injected at specific amplifier locations, whereas the dominant PDL hinges are associated with WSSs and other localized components. Their relative longitudinal arrangement is therefore highly asymmetric, and the q_i coefficients in (17) are strongly non-uniform. As a result, reversing a path or changing the receiver operating point does not merely translate a fixed PDF: it changes which noise contributions are filtered by which portions of the PDL cascade, leading to more structured and potentially more skewed PDL-induced SNR distributions.

A. Core–Metro Network

The first application joins the 500-km core section to the metro section and evaluates both propagation directions. For the core–metro and metro–core cases, the gain plan is assumed to fully recover the transmitted optical power at the receiver. The received optical power (ROP) is consequently 3 dBm in total over the two polarizations, or approximately 0 dBm per polarization axis, and the transceiver SNR is $\mathrm{SNR}_{\mathrm{TRX}} = 22$ dB. Thus, the two directions have the same transmitter and receiver operating point and differ primarily in the longitudinal ordering of the core and metro resources.

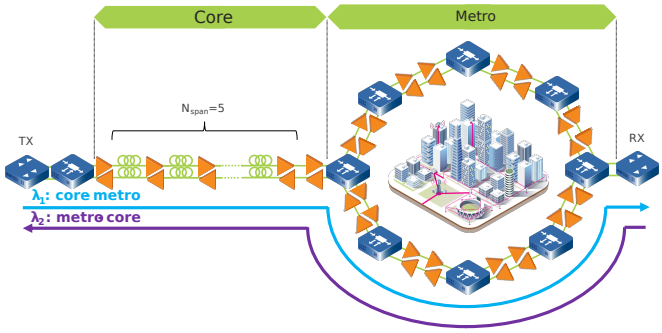

FIGURE 5. Core–metro network scenario used for the realistic application study.

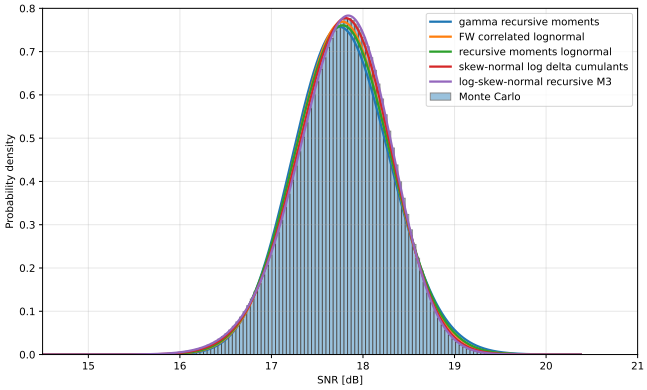

FIGURE 6. PDL-induced SNR distribution for the core–metro direction, with total ROP 3 dBm and $\mathrm{SNR}_{\mathrm{TRX}} = 22$ dB.

TABLE 4. Core–metro approximation metrics under realistic non-uniform noise loading. The case uses $N = 6$, $\sigma_{\mathrm{PDL}} = 0.5\,\mathrm{dB}$, total ROP 3 dBm (0 dBm per polarization axis), and $\mathrm{SNR}_{\mathrm{TRX}} = 22$ dB.

Approximation	KS	RMSE	KL	$\mathrm{RMSE}_{\log_{10}(P_{\mathrm{out}})}$	$\mathrm{RMSE}_{Q,\mathrm{dB}}$
Gamma	0.0233	9.69e-04	0.0106	2.393	0.503
FW correlated	0.0153	6.29e-04	0.0045	1.546	0.368
Lognormal recursive	0.0154	6.45e-04	0.0047	1.425	0.344
Log-skew-normal Δ_3	0.0068	2.75e-04	9.33e-04	0.604	0.175
Log-skew-normal M3	0.0016	8.94e-05	9.06e-05	0.189	0.058

TABLE 5. Metro–core approximation metrics under realistic non-uniform noise loading. The case uses $N = 6$, $\sigma_{\mathrm{PDL}} = 0.5\,\mathrm{dB}$, total ROP 3 dBm (0 dBm per polarization axis), and $\mathrm{SNR}_{\mathrm{TRX}} = 22$ dB.

Approximation	KS	RMSE	KL	$\mathrm{RMSE}_{\log_{10}(P_{\mathrm{out}})}$	$\mathrm{RMSE}_{Q,\mathrm{dB}}$
Gamma	0.0204	8.65e-04	0.0084	2.207	0.613
FW correlated	0.0082	3.37e-04	0.0013	0.774	0.296
Lognormal recursive	0.0081	3.50e-04	0.0014	0.670	0.260
Log-skew-normal Δ_3	0.0013	5.84e-05	4.76e-05	0.071	0.031
Log-skew-normal M3	0.0010	5.09e-05	3.44e-05	0.043	0.019

Figures 6 and 7 show that reversing the same classes of resources changes the PDL-induced SNR law even though the ROP and $\mathrm{SNR}_{\mathrm{TRX}}$ are unchanged. The difference is therefore a direct signature of the non-commutative longitudinal interleaving of ASE and PDL. Tables 4 and 5 also show that the third-moment recursive log-skew-normal

This work is licensed under a Creative Commons Attribution 4.0 License. For more information, see https://creativecommons.org/licenses/by/4.0/

This article has been accepted for publication in IEEE Open Journal of the Communications Society. This is the author's version which has not been fully edited and content may change prior to final publication. Citation information: DOI 10.1109/OJCOMS.2026.3741461

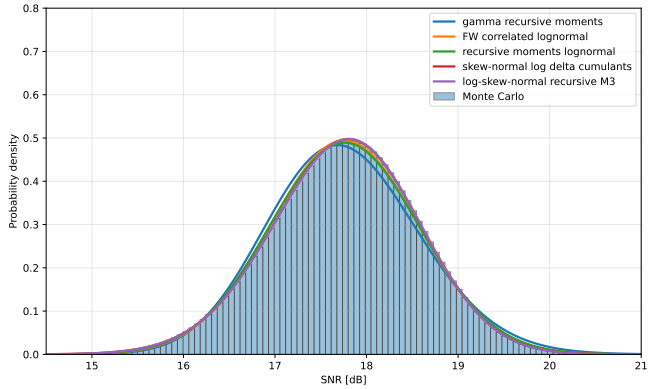

FIGURE 7. PDL-induced SNR distribution for the reverse metro–core direction, with total ROP 3 dBm and $\mathrm{SNR}_{\mathrm{TRX}} = 22$ dB.

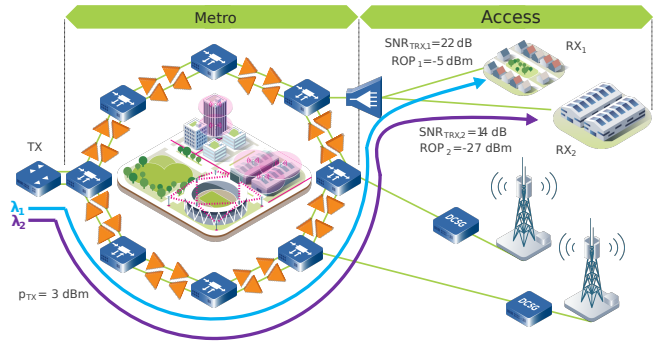

FIGURE 8. Metro–access scenario used to study the interaction between access attenuation, receiver operating power, transceiver noise, and PDL.

approximation remains the most accurate in both directions. Its outage-probability RMSE is 0.189 decades with a 0.058-dB outage-quantile RMSE in the core–metro direction, and it improves to 0.043 decades and 0.019 dB in the reverse direction. By contrast, the gamma approximation exceeds two decades of outage-probability error in both cases, while the two-moment lognormal approximations are especially challenged in the core–metro direction. The fact that the relative ranking and absolute errors depend on propagation direction confirms that realistic non-uniform loading produces more difficult PDF shapes than the translation-invariant benchmark of Section VII.

B. Metro–Access Network

The second application considers a metro–access lightpath with the same 3 dBm total dual-polarization transmitted power. The access-network attenuation changes the receiver operating point in two cases. In Case 1, representing the lower attenuation, the total ROP is -5 dBm and $\mathrm{SNR}_{\mathrm{TRX}} = 22$ dB; the corresponding per-polarization ROP is approximately -8 dBm. In Case 2, representing the higher attenuation, the total ROP is -27 dBm and $\mathrm{SNR}_{\mathrm{TRX}} = 14$ dB; the corresponding per-polarization ROP is approximately -30 dBm. The metro line-system parameters remain those stated above, so the comparison isolates the combined consequence of access attenuation and transceiver operating condition while retaining the realistic non-uniform line-noise profile.

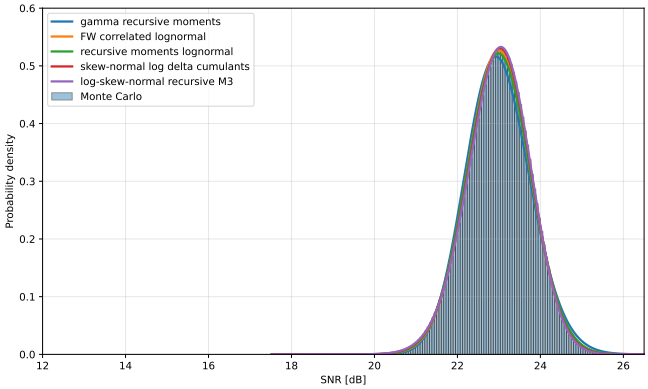

FIGURE 9. Metro–access PDL-induced SNR distribution, Case 1 (lower access attenuation): total ROP -5 dBm and $\mathrm{SNR}_{\mathrm{TRX}} = 22$ dB.

TABLE 6. Metro–access Case 1 approximation metrics under realistic non-uniform noise loading. The case uses $N = 6$, $\sigma_{\mathrm{PDL}} = 0.5\,\mathrm{dB}$, total ROP -5 dBm (-8 dBm per polarization axis), and $\mathrm{SNR}_{\mathrm{TRX}} = 22$ dB.

Approximation	KS	RMSE	KL	$\mathrm{RMSE}_{\log_{10}(P_{\mathrm{out}})}$	$\mathrm{RMSE}_{Q,\mathrm{dB}}$
Gamma	0.0216	9.06e-04	0.0094	2.271	0.616
FW correlated	0.0101	4.14e-04	0.0020	0.939	0.335
Lognormal recursive	0.0101	4.29e-04	0.0022	0.831	0.301
Log-skew-normal Δ_3	0.0033	1.32e-04	2.34e-04	0.226	0.096
Log-skew-normal M3	0.0012	6.21e-05	5.14e-05	0.052	0.022

TABLE 7. Metro–access Case 2 approximation metrics under realistic non-uniform noise loading. The case uses $N = 6$, $\sigma_{\mathrm{PDL}} = 0.5\,\mathrm{dB}$, total ROP -27 dBm (-30 dBm per polarization axis), and $\mathrm{SNR}_{\mathrm{TRX}} = 14$ dB.

Approximation	KS	RMSE	KL	$\mathrm{RMSE}_{\log_{10}(P_{\mathrm{out}})}$	$\mathrm{RMSE}_{Q,\mathrm{dB}}$
Gamma	0.0209	8.81e-04	0.0089	2.234	0.662
FW correlated	0.0078	3.15e-04	0.0011	0.713	0.297
Lognormal recursive	0.0076	3.28e-04	0.0013	0.611	0.258
Log-skew-normal Δ_3	0.0012	5.45e-05	4.24e-05	0.048	0.023
Log-skew-normal M3	0.0010	4.80e-05	3.16e-05	0.023	0.011

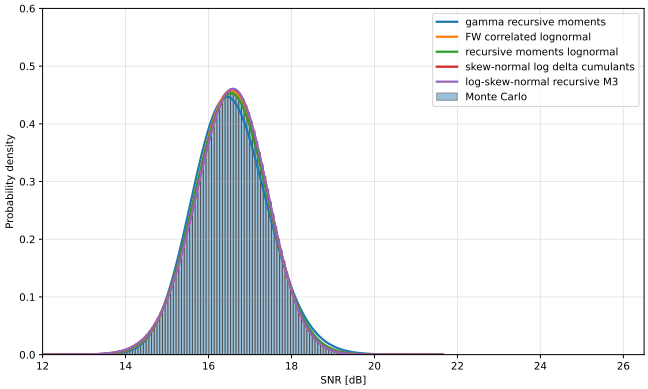

FIGURE 10. Metro–access PDL-induced SNR distribution, Case 2 (higher access attenuation): total ROP -27 dBm and $\mathrm{SNR}_{\mathrm{TRX}} = 14$ dB.

This work is licensed under a Creative Commons Attribution 4.0 License. For more information, see https://creativecommons.org/licenses/by/4.0/

This article has been accepted for publication in IEEE Open Journal of the Communications Society. This is the author's version which has not been fully edited and content may change prior to final publication. Citation information: DOI 10.1109/OJCOMS.2026.3741461

TABLE 8. Paired ablation averaged over the four realistic application cases. Lower values are better.

Model	Mean outage error (decades)	Mean quantile error (dB)
Recursive lognormal (two raw moments)	0.884	0.291
Log-skew-normal Δ_3 (log cumulants)	0.237	0.081
Log-skew-normal M3 (three raw moments)	0.077	0.028

The third-moment recursive log-skew-normal model again gives the best overall agreement. In Case 1, its outage-probability and outage-quantile RMSEs are 0.052 decades and 0.022 dB, respectively; in Case 2 they are 0.023 decades and 0.011 dB. The smaller approximation error in Case 2 must not be interpreted as better transmission performance: the entire SNR distribution is referenced to a much lower ROP and to a transceiver SNR reduced from 22 to 14 dB. Comparing Figures 9 and 10, the transceiver operating point and access loss change not only the location of the distribution but also its width and shape. In the inverse-SNR representation, the transceiver contribution changes the deterministic reference term, while the PDL-impaired line contribution remains random; changing their relative weights modifies the nonlinear mapping from Y_N to SNR. Therefore, a PDL margin obtained for one ROP or one $\mathrm{SNR}_{\mathrm{TRX}}$ cannot, in general, be reused through a simple SNR translation. The interaction between PDL and transceiver performance is pivotal for a realistic and accurate margin assessment.

C. Paired Ablation of Skewness and Moment Information

The comparison between the recursive lognormal and third-moment recursive log-skew-normal changes both the available moment information and the distribution family. To clarify the source of the improvement, Table 8 reports an unweighted mean over the four realistic cases in Tables 4–7. The first transition, from the two-moment recursive lognormal to the delta-cumulant log-skew-normal, introduces a skew-capable third-order log-domain description. The second transition keeps the log-skew-normal family fixed and replaces the local log-delta cumulants with the exact finite-cascade raw moments through order three.

Relative to the recursive lognormal, the delta-cumulant log-skew-normal reduces the two mean errors by approximately 73% and 72%, respectively. Within the same log-skew-normal family, replacing the delta construction with exact third-raw-moment recursion yields a further reduction of approximately 68% and 66%. Most of the absolute improvement over the two-moment baseline therefore appears when a skew-capable third-order description is introduced, while exact finite-cascade third-moment information supplies an additional gain. These comparisons do not separate distribution family and moment order as fully independent factors, because the three-parameter log-skew-normal law requires a third identifying constraint. They nevertheless show that the M3 advantage is not caused only by choosing a skewed family, since the same-family Δ_3 model remains less accurate.

Taken together, the core–metro and metro–access applications show that the proposed approximations remain promising across the four representative profiles considered, which include realistic span losses, WSS insertion losses, amplifier NFs, direction-dependent noise placement, and receiver operating points. They also reinforce the central ONDT requirement: the outage margin must be evaluated from the actual ordered lightpath description, or from a compact domain descriptor that preserves its moment evolution, rather than from total loss, total ASE, total PDL, and transceiver specifications considered separately.

D. Scope of the Numerical Validation

The validation in Section VII is exhaustive with respect to the stated grid for uniformly distributed ASE: every combination of $N \in \{2, 10, 40\}$ and $\sigma_{\mathrm{PDL}} \in [0.1, 1.5]$ dB in 0.05-dB steps is evaluated by Monte Carlo simulation and with all five approximation families. This coverage should not be interpreted as exhaustive validation over arbitrary longitudinal ASE profiles. The four non-uniform cases in this section are representative application studies intended to remove the uniform-loading symmetry and test the approach under ordered core–metro and metro–access configurations. They do not span the full range of amplifier locations, span losses, receiver operating powers, transceiver-noise levels, or heterogeneous device priors. A systematic campaign over those dimensions would require a substantially larger study and is left for future work.

IX. CONCLUSION

This paper developed an outage-aware statistical description of the post-equalization SNR of coherent links containing finite, localized PDL elements and distributed additive noise. The finite-hinge model reduces the random inverse-SNR to a weighted sum of correlated exponentials of a random walk, retaining the longitudinal ordering that is lost in end-to-end PDL or total-noise summaries. Five low-complexity approximations were formulated and compared. Their required moments or cumulants can be accumulated in linear time and converted directly into a POOS or an outage quantile, making the framework suitable for repeated ONDT evaluation.

The Monte Carlo campaign showed that no elementary distribution is uniformly optimal over every cascade length and every per-element PDL variance. The gamma model is simple but generally too inaccurate in the outage tail, while the two-moment lognormal approaches reproduce the scale better but have limited control of asymmetry. The delta-cumulant log-skew-normal model is more regular in the very high-PDL portion of the sweep. In the sub-1 dB range that more closely represents measured device-level variability, however, the third-moment recursive log-skew-normal approximation provides the best overall compromise:

This work is licensed under a Creative Commons Attribution 4.0 License. For more information, see https://creativecommons.org/licenses/by/4.0/

This article has been accepted for publication in IEEE Open Journal of the Communications Society. This is the author's version which has not been fully edited and content may change prior to final publication. Citation information: DOI 10.1109/OJCOMS.2026.3741461

it is generally the most accurate global model and gives the smallest outage-probability and outage-quantile errors. Its degradation for very large σ_{PDL}, where $\mathbb{E}[A^{-3}]$ becomes dominated by rare near-singular gains, is an important limitation rather than a reason to extrapolate the model without checking its regime of validity.

The representative core–metro and metro–access studies further illustrate why this distributional treatment is needed. The same nominal resources produce different PDFs when their propagation order is reversed, because ASE sources and PDL hinges are strongly and asymmetrically interleaved. In the access cases, changing the ROP and $\mathrm{SNR}_{\mathrm{TRX}}$ modifies both the reference SNR and the width and shape of the distribution. Consequently, the transceiver contribution and the PDL-impaired line cannot be assigned independent fixed margins and then combined by a simple translation. The third-moment recursive log-skew-normal model retained the best tail accuracy in all four cases. These results support the promise of the approach under non-uniform loading, but they do not constitute an exhaustive validation over arbitrary longitudinal ASE profiles.

For multi-vendor and multi-operator deployment, different network portions may use different $\sigma_{\mathrm{PDL},i}$ values or different device-level priors. The proposed recursion already supports this heterogeneity. Moreover, a federated implementation can pass only a constant-size moment state between domains, together with the power normalization, endpoint transceiver term, and operating metadata, rather than disclosing the complete internal topology. Total PDL variance and total ASE alone are not sufficient because they do not preserve longitudinal ordering.

The present scope remains restricted to ASE-dominated operation, independent per-element Maxwell PDL priors, ideal compensation of chromatic dispersion, and ideal 2×2 zero-forcing polarization equalization. Future work should incorporate Kerr nonlinear-noise statistics, residual chromatic dispersion, PMD–PDL frequency dependence, MMSE and implementation-aware receivers, correlations among device PDL values and operating states, measurement-conditioned or time-varying priors, systematic validation over non-uniform longitudinal ASE profiles, uncertainty propagation for coarse inter-domain descriptors, and experimental validation of the proposed federated exchange on multi-vendor lightpaths.

References

[1] E. Agrell et al., "Roadmap on optical communications," *Journal of Optics*, vol. 26, no. 9, p. 093 001, Jul. 2024, ISSN: 2040-8986. DOI: 10.1088/2040-8986/ad261f. Accessed: Jul. 28, 2026. [Online]. Available: https://doi.org/10.1088/2040-8986/ad261f.

[2] I. Tomkos, S. Azodolmolky, J. Solé-Pareta, D. Careglio, and E. Palkopoulou, "A tutorial on the flexible optical networking paradigm: State of the art, trends, and research challenges," *Proceedings of the IEEE*, vol. 102, no. 9, pp. 1317–1337, Sep. 2014, ISSN: 1558-2256. DOI: 10.1109/JPROC.2014.2324652. Accessed: Jul. 28, 2026. [Online]. Available: https://ieeexplore.ieee.org/document/6824237.

[3] K. Roberts, Q. Zhuge, I. Monga, S. Gareau, and C. Laperle, "Beyond 100 gb/s: Capacity, flexibility, and network optimization [invited]," *Journal of Optical Communications and Networking*, vol. 9, no. 4, pp. C12–C23, Apr. 2017, ISSN: 1943-0639. DOI: 10.1364/JOCN.9.000C12. Accessed: Jul. 28, 2026. [Online]. Available: https://ieeexplore.ieee.org/document/7901442.

[4] A. Lord, S. J. Savory, M. Tornatore, and A. Mitra, "Flexible technologies to increase optical network capacity," *Proceedings of the IEEE*, vol. 110, no. 11, pp. 1714–1724, Nov. 2022, ISSN: 1558-2256. DOI: 10.1109/JPROC.2022.3188337. Accessed: Jul. 28, 2026. [Online]. Available: https://ieeexplore.ieee.org/document/9833809.

[5] M. Imran, P. M. Anandarajah, A. Kaszubowska-Anandarajah, N. Sambo, and L. Potí, "A survey of optical carrier generation techniques for terabit capacity elastic optical networks," *IEEE Communications Surveys & Tutorials*, vol. 20, no. 1, pp. 211–263, 2018, ISSN: 1553-877X. DOI: 10.1109/COMST.2017.2775039. Accessed: Jul. 28, 2026. [Online]. Available: https://ieeexplore.ieee.org/document/8114183.

[6] H. Nishizawa et al., "Dynamic optical path provisioning for alien access links: Architecture, demonstration, and challenges," *IEEE Communications Magazine*, vol. 61, no. 12, pp. 84–90, 2023. DOI: 10.1109/MCOM.001.2200660.

[7] J. Müller et al., "Physical-layer-aware multi-band optical network planning framework for rate-adaptive transceivers," *Journal of Optical Communications and Networking*, vol. 16, no. 5, B71, May 1, 2024, ISSN: 1943-0620, 1943-0639. DOI: 10.1364/JOCN.514026. Accessed: Jul. 28, 2026. [Online]. Available: https://opg.optica.org/abstract.cfm?URI=jocn-16-5-B71.

[8] V. Curri, "GNPy model of the physical layer for open and disaggregated optical networking [invited]," *Journal of Optical Communications and Networking*, vol. 14, no. 6, pp. C92–C104, Jun. 2022, ISSN: 1943-0639. DOI: 10.1364/JOCN.452868. Accessed: Jul. 28, 2026. [Online]. Available: https://ieeexplore.ieee.org/document/9768871.

[9] H. Nishizawa et al., *Optical network digital twin – practical use cases and architecture*, arXiv preprint, Available: https://arxiv.org/abs/2511.06368, 2025.

[10] Y. Pointurier, "Design of low-margin optical networks," *Journal of Optical Communications and Networking*, vol. 9, no. 1, A9, Jan. 1, 2017, ISSN: 1943-0620, 1943-0639. DOI: 10.1364/JOCN.9.0000A9. Accessed: Jul. 28, 2026. [Online]. Available: https://opg.optica.org/abstract.cfm?URI=jocn-9-1-A9.

This work is licensed under a Creative Commons Attribution 4.0 License. For more information, see https://creativecommons.org/licenses/by/4.0/

This article has been accepted for publication in IEEE Open Journal of the Communications Society. This is the author's version which has not been fully edited and content may change prior to final publication. Citation information: DOI 10.1109/OJCOMS.2026.3741461

[11] D. W. Boertjes, M. Reimer, and D. Côté, "Practical considerations for near-zero margin network design and deployment [invited]," *Journal of Optical Communications and Networking*, vol. 11, no. 9, p. C25, Sep. 1, 2019, ISSN: 1943-0620, 1943-0639. DOI: 10.1364/JOCN.11.000C25. Accessed: Jul. 28, 2026. [Online]. Available: https://opg.optica.org/abstract.cfm?URI=jocn-11-9-C25.

[12] M. Filer, J. Gaudette, Y. Yin, D. Billor, Z. Bakhtiari, and J. L. Cox, "Low-margin optical networking at cloud scale [invited]," *Journal of Optical Communications and Networking*, vol. 11, no. 10, pp. C94–C108, Oct. 1, 2019, ISSN: 1943-0639. DOI: 10.1364/JOCN.11.000C94. Accessed: Jul. 28, 2026. [Online]. Available: https://opg.optica.org/jocn/abstract.cfm?uri=jocn-11-10-C94.

[13] M. Shtaif, "Performance degradation in coherent polarization multiplexed systems as a result of polarization dependent loss," *Optics Express*, vol. 16, no. 18, pp. 13 918–13 932, Sep. 1, 2008, ISSN: 1094-4087. DOI: 10.1364/OE.16.013918. Accessed: Jul. 28, 2026. [Online]. Available: https://opg.optica.org/oe/abstract.cfm?uri=oe-16-18-13918.

[14] Z. Tao, L. Dou, T. Hoshida, and J. C. Rasmussen, "A fast method to simulate the PDL impact on dual-polarization coherent systems," *IEEE Photonics Technology Letters*, vol. 21, no. 24, pp. 1882–1884, Dec. 2009, ISSN: 1941-0174. DOI: 10.1109/LPT.2009.2034984. Accessed: Jul. 28, 2026. [Online]. Available: https://ieeexplore.ieee.org/document/5291798.

[15] E. Miotto, A. D'Amico, S. Straullu, T. Mano, H. Nishizawa, and V. Curri, "Exact PDL-induced SNR statistics in dual-polarization coherent optical communication systems," *Optics Express*, vol. 34, no. 11, p. 19 588, Jun. 1, 2026, ISSN: 1094-4087. DOI: 10.1364/OE.587873. Accessed: Jul. 23, 2026. [Online]. Available: https://opg.optica.org/abstract.cfm?URI=oe-34-11-19588.

[16] A. D'Amico et al., "Statistical analysis of PDL penalty on coherent transmission technologies based on WSS experimental characterization," in *2022 Asia Communications and Photonics Conference (ACP)*, Shenzhen, China: IEEE, Nov. 5, 2022, pp. 874–877, ISBN: 978-1-6654-8155-7. DOI: 10.1109/ACP55869.2022.10088670. Accessed: Jul. 23, 2026. [Online]. Available: https://ieeexplore.ieee.org/document/10088670/.

[17] G. Borraccini et al., "On the characterization of PDL distribution in wavelength selective switches," in *2023 IEEE Photonics Conference (IPC)*, ISSN: 2575-274X, Nov. 2023, pp. 1–2. DOI: 10.1109/IPC57732.2023.10360707. Accessed: Jul. 28, 2026. [Online]. Available: https://ieeexplore.ieee.org/abstract/document/10360707.

[18] E. Miotto, A. D'Amico, R. Ambrosone, F. Aquilino, S. Straullu, and V. Curri, "Statistical assessment of system margin in metro networks impaired by PDL," in *2025 Optical Fiber Communications Conference and Exhibition (OFC)*, Mar. 2025, pp. 1–3. Accessed: Jul. 23, 2026. [Online]. Available: https://ieeexplore.ieee.org/abstract/document/11046914.

[19] S. Zarkosvky and M. Shtaif, "Statistical distribution of polarization-dependent loss in systems characterized by the hinge model," *Optics Letters*, vol. 45, no. 5, pp. 1224–1227, Mar. 1, 2020, ISSN: 1539-4794. DOI: 10.1364/OL.385525. Accessed: Jul. 28, 2026. [Online]. Available: https://opg.optica.org/ol/abstract.cfm?uri=ol-45-5-1224.

[20] G. Taricco, "On the convergence of multipath fading channel gains to the rayleigh distribution," *IEEE Wireless Communications Letters*, vol. 4, no. 5, pp. 549–552, 2015. DOI: 10.1109/LWC.2015.2456066.

[21] L. Fenton, "The sum of log-normal probability distributions in scatter transmission systems," *IRE Transactions on Communications Systems*, vol. 8, no. 1, pp. 57–67, 1960.

[22] A. Azzalini, "A class of distributions which includes the normal ones," *Scandinavian Journal of Statistics*, vol. 12, no. 2, pp. 171–178, 1985.

[23] B. Mukherjee, I. Tomkos, M. Tornatore, P. Winzer, and Y. Zhao, Eds., *Springer Handbook of Optical Networks*, Springer Handbooks, Cham: Springer International Publishing, 2020, ISBN: 978-3-030-16250-4. DOI: 10.1007/978-3-030-16250-4. Accessed: Jul. 28, 2026. [Online]. Available: https://link.springer.com/10.1007/978-3-030-16250-4.

[24] R. Casellas, A. Giorgetti, R. Morro, R. Martínez, R. Vilalta, and R. Muñoz, "Enabling network slicing across a disaggregated optical transport network," in *2019 Optical Fiber Communications Conference and Exhibition (OFC)*, Mar. 2019, pp. 1–3. Accessed: Jul. 28, 2026. [Online]. Available: https://ieeexplore.ieee.org/document/8696776.

[25] R. Casellas, A. Giorgetti, R. Morro, R. Martinez, R. Vilalta, and R. Munoz, "Virtualization of disaggregated optical networks with open data models in support of network slicing," *Journal of Optical Communications and Networking*, vol. 12, no. 2, A144–A154, Feb. 2020, ISSN: 1943-0639. DOI: 10.1364/JOCN.12.00A144. Accessed: Jul. 28, 2026. [Online]. Available: https://ieeexplore.ieee.org/document/8897693.

[26] J.-i. Kani, "Disaggregation and virtualization for future access and metro networks," in *Optical Fiber Communication Conference (OFC) 2024*, San Diego California: Optica Publishing Group, 2024, Tu3I.2, ISBN: 978-1-957171-32-6. DOI: 10.1364/OFC.2024.Tu3I.2. Accessed: Jul. 28, 2026. [Online]. Available: https://opg.optica.org/abstract.cfm?URI=OFC-2024-Tu3I.2.

[27] J.-i. Kani, T. Suzuki, Y. Kimura, S. Kaneko, S.-Y. Kim, and T. Yoshida, "Disaggregation and virtualiza-

This work is licensed under a Creative Commons Attribution 4.0 License. For more information, see https://creativecommons.org/licenses/by/4.0/

This article has been accepted for publication in IEEE Open Journal of the Communications Society. This is the author's version which has not been fully edited and content may change prior to final publication. Citation information: DOI 10.1109/OJCOMS.2026.3741461

tion for future access and metro networks [invited tutorial]," *Journal of Optical Communications and Networking*, vol. 17, no. 1, A1–A12, Jan. 2025, ISSN: 1943-0639. DOI: 10.1364/JOCN.534303. Accessed: Jul. 28, 2026. [Online]. Available: https://ieeexplore.ieee.org/document/10734083.

[28] D. Wang et al., "The role of digital twin in optical communication: Fault management, hardware configuration, and transmission simulation," *IEEE Communications Magazine*, vol. 59, no. 1, pp. 133–139, Jan. 2021, ISSN: 1558-1896. DOI: 10.1109/MCOM.001.2000727. Accessed: Jul. 28, 2026. [Online]. Available: https://ieeexplore.ieee.org/document/9356524.

[29] Q. Zhuge et al., "Building a digital twin for intelligent optical networks [invited tutorial]," *Journal of Optical Communications and Networking*, vol. 15, no. 8, pp. C242–C262, Aug. 2023, ISSN: 1943-0639. DOI: 10.1364/JOCN.483600. Accessed: Jul. 28, 2026. [Online]. Available: https://ieeexplore.ieee.org/document/10187397/.

[30] M. S. Faruk and S. J. Savory, "Measurement informed models and digital twins for optical fiber communication systems," *Journal of Lightwave Technology*, vol. 42, no. 3, pp. 1016–1030, Feb. 2024, ISSN: 1558-2213. DOI: 10.1109/JLT.2023.3328765. Accessed: Jul. 28, 2026. [Online]. Available: https://ieeexplore.ieee.org/document/10304066.

[31] D. Wang et al., "Digital twin of optical networks: A review of recent advances and future trends," *Journal of Lightwave Technology*, vol. 42, no. 12, pp. 4233–4259, Jun. 15, 2024. Accessed: Jul. 28, 2026. [Online]. Available: https://opg.optica.org/jlt/abstract.cfm?uri=jlt-42-12-4233.

[32] Q. Zhuge, "Optical fiber communication conference (OFC) tutorial, w4g.1 april 2, 2025," 2025.

[33] S. Cruzes, "Telemetry and agentic AI: Foundations for optical network automation," *IEEE Access*, vol. 14, pp. 8800–8838, 2026, ISSN: 2169-3536. DOI: 10.1109/ACCESS.2025.3649768. Accessed: Jul. 28, 2026. [Online]. Available: https://ieeexplore.ieee.org/document/11318586.

[34] H. Nishizawa et al., "Leveraging digital twin technologies: All-photonics networks-as-a-service for data center xchange in the era of AI [invited tutorial]," *Journal of Optical Communications and Networking*, vol. 18, no. 7, pp. C49–C65, Jul. 1, 2026, ISSN: 1943-0639. DOI: 10.1364/JOCN.590102. Accessed: Jul. 28, 2026. [Online]. Available: https://opg.optica.org/jocn/abstract.cfm?uri=jocn-18-7-C49.

[35] T. A. Strasser and J. L. Wagener, "Wavelength-selective switches for ROADM applications," *IEEE Journal of Selected Topics in Quantum Electronics*, vol. 16, no. 5, pp. 1150–1157, Sep. 2010, ISSN: 1558-4542. DOI: 10.1109/JSTQE.2010.2049345. Accessed: Jul. 28, 2026. [Online]. Available: https://ieeexplore.ieee.org/document/5512667.

[36] Y. Ma, L. Stewart, J. Armstrong, I. G. Clarke, and G. Baxter, "Recent progress of wavelength selective switch," *Journal of Lightwave Technology*, vol. 39, no. 4, pp. 896–903, Feb. 2021, ISSN: 1558-2213. DOI: 10.1109/JLT.2020.3022375. Accessed: Jul. 28, 2026. [Online]. Available: https://ieeexplore.ieee.org/document/9187937.

[37] F. Bruyere and O. Audouin, "Penalties in long-haul optical amplifier systems due to polarization dependent loss and gain," *IEEE Photonics Technology Letters*, vol. 6, no. 5, pp. 654–656, May 1994, ISSN: 1941-0174. DOI: 10.1109/68.285570. Accessed: Jul. 28, 2026. [Online]. Available: https://ieeexplore.ieee.org/document/285570.

[38] Q. Wang, G. Rajan, P. Wang, and G. Farrell, "Polarization dependence of bend loss for a standard singlemode fiber," *Optics Express*, vol. 15, no. 8, pp. 4909–4920, Apr. 16, 2007, ISSN: 1094-4087. DOI: 10.1364/OE.15.004909. Accessed: Jul. 28, 2026. [Online]. Available: https://opg.optica.org/oe/abstract.cfm?uri=oe-15-8-4909.

[39] L. E. Nelson et al., "Statistics of polarization dependent loss in an installed long-haul WDM system," *Optics Express*, vol. 19, no. 7, pp. 6790–6796, Mar. 28, 2011, ISSN: 1094-4087. DOI: 10.1364/OE.19.006790. Accessed: Jul. 28, 2026. [Online]. Available: https://opg.optica.org/oe/abstract.cfm?uri=oe-19-7-6790.

[40] I. Kaminow, "Polarization in optical fibers," *IEEE Journal of Quantum Electronics*, vol. 17, no. 1, pp. 15–22, Jan. 1981, ISSN: 1558-1713. DOI: 10.1109/JQE.1981.1070626. Accessed: Jul. 28, 2026. [Online]. Available: https://ieeexplore.ieee.org/document/1070626.

[41] A. Dumenil, E. Awwad, and C. Measson, "Rate optimization using SO(4) transforms for PDL mitigation," in *45th European Conference on Optical Communication (ECOC 2019)*, Sep. 2019, pp. 1–4. DOI: 10.1049/cp.2019.0927. Accessed: Jul. 28, 2026. [Online]. Available: https://ieeexplore.ieee.org/document/9125655.

[42] A. Dumenil, E. Awwad, and C. Méasson, "PDL in optical links: A model analysis and a demonstration of a PDL-resilient modulation," *Journal of Lightwave Technology*, vol. 38, no. 18, pp. 5017–5025, Sep. 2020, ISSN: 1558-2213. DOI: 10.1109/JLT.2020.2998841. Accessed: Jul. 28, 2026. [Online]. Available: https://ieeexplore.ieee.org/document/9104875.

[43] C. Zhu, B. Song, B. Corcoran, L. Zhuang, and A. J. Lowery, "Improved polarization dependent loss tolerance for polarization multiplexed coherent optical systems by polarization pairwise coding," *Optics Express*, vol. 23, no. 21, p. 27 434, Oct. 19, 2015, ISSN: 1094-4087. DOI: 10.1364/OE.23.027434. Accessed:

This work is licensed under a Creative Commons Attribution 4.0 License. For more information, see https://creativecommons.org/licenses/by/4.0/

This article has been accepted for publication in IEEE Open Journal of the Communications Society. This is the author's version which has not been fully edited and content may change prior to final publication. Citation information: DOI 10.1109/OJCOMS.2026.3741461

Jul. 28, 2026. [Online]. Available: https://opg.optica.org/abstract.cfm?URI=oe-23-21-27434.

[44] C. Delezoide, H. Akbari, P. Ramantanis, F. Boitier, and P. Layec, "On the detection, modeling, and mitigation of anomalous QoT fluctuations in optical networks," *Journal of Optical Communications and Networking*, vol. 16, no. 5, B35–B44, May 2024, ISSN: 1943-0639. DOI: 10.1364/JOCN.514779. Accessed: Jul. 28, 2026. [Online]. Available: https://ieeexplore.ieee.org/document/10494035/.

[45] A. D'Amico et al., "Experimental probing and modeling of the PDL impact on the optical signal-to-noise ratio," in *Optical Fiber Communication Conference (OFC) 2023 (2023), paper W1E.6*, Optica Publishing Group, Mar. 5, 2023, W1E.6. DOI: 10.1364/OFC.2023.W1E.6. Accessed: Jul. 28, 2026. [Online]. Available: https://opg.optica.org/abstract.cfm?uri=OFC-2023-W1E.6.

[46] J. Girard-Jollet et al., "Estimating network components polarization-dependent loss using performance statistical measurements," in *2021 European Conference on Optical Communication (ECOC)*, Sep. 2021, pp. 1–4. DOI: 10.1109/ECOC52684.2021.9606155. Accessed: Jul. 28, 2026. [Online]. Available: https://ieeexplore.ieee.org/document/9606155.

[47] J. Girard-Jollet et al., "Estimating network components PDL using performance statistical measurements," *Journal of Lightwave Technology*, vol. 40, no. 16, pp. 5407–5415, Aug. 2022, ISSN: 1558-2213. DOI: 10.1109/JLT.2022.3181786. Accessed: Jul. 28, 2026. [Online]. Available: https://ieeexplore.ieee.org/document/9794439.

[48] M. Takahashi, T. Sasai, E. Yamazaki, and Y. Kisaka, "Monitoring PDL value and location using DSP-based longitudinal power profile estimation," *Journal of Lightwave Technology*, vol. 42, no. 17, pp. 5866–5873, Sep. 2024, ISSN: 1558-2213. DOI: 10.1109/JLT.2024.3407722. Accessed: Jul. 28, 2026. [Online]. Available: https://ieeexplore.ieee.org/document/10543040/.

[49] E. Seve, F. Boitier, P. Ramantanis, L. Shi, and P. Layec, "Localization and estimation of multiple PDL anomalies by monitoring a single SNR distribution at the receiver side," in *2025 European Conference on Optical Communications (ECOC)*, Sep. 2025, pp. 1–4. DOI: 10.1109/ECOC66593.2025.11263058. Accessed: Jul. 28, 2026. [Online]. Available: https://ieeexplore.ieee.org/document/11263058/.

[50] B. Huttner, C. Geiser, and N. Gisin, "Polarization-induced distortions in optical fiber networks with polarization-mode dispersion and polarization-dependent losses," *IEEE Journal of Selected Topics in Quantum Electronics*, vol. 6, no. 2, pp. 317–329, Mar. 2000, ISSN: 1558-4542. DOI: 10.1109/2944.847767. Accessed: Jul. 28, 2026. [Online]. Available: https://ieeexplore.ieee.org/document/847767.

[51] A. Mecozzi and M. Shtaif, "The statistics of polarization-dependent loss in optical communication systems," *IEEE Photonics Technology Letters*, vol. 14, no. 3, pp. 313–315, Mar. 2002, ISSN: 1941-0174. DOI: 10.1109/68.986797. Accessed: Jul. 28, 2026. [Online]. Available: https://ieeexplore.ieee.org/document/986797.

[52] A. Galtarossa and L. Palmieri, "The exact statistics of polarization-dependent loss in fiber-optic links," *IEEE Photonics Technology Letters*, vol. 15, no. 1, pp. 57–59, Jan. 2003, ISSN: 1941-0174. DOI: 10.1109/LPT.2002.805799. Accessed: Jul. 28, 2026. [Online]. Available: https://ieeexplore.ieee.org/document/1159061/.

[53] X. Lin and Z. Jiang, "Generalized probability density function of polarization-dependent loss in optical links," *IEEE Photonics Technology Letters*, vol. 36, no. 2, pp. 79–82, Jan. 2024, ISSN: 1941-0174. DOI: 10.1109/LPT.2023.3336211. Accessed: Jul. 28, 2026. [Online]. Available: https://ieeexplore.ieee.org/document/10330697.

[54] J. Cartledge and A. I. Abd El-Rahman, "Estimating the outage probability due to polarization dependent loss using threshold exceedances," *Journal of Lightwave Technology*, vol. 39, no. 1, pp. 136–145, Jan. 2021, ISSN: 1558-2213. DOI: 10.1109/JLT.2020.3024057. Accessed: Jul. 28, 2026. [Online]. Available: https://ieeexplore.ieee.org/document/9198069.

[55] M. Shtaif, A. Mecozzi, and R. Tkach, "Noise enhancement caused by polarization dependent loss and the effect of dynamic gain equalizers," in *Optical Fiber Communication Conference and Exhibit*, Mar. 2002, pp. 48–50. DOI: 10.1109/OFC.2002.1036195. Accessed: Jul. 28, 2026. [Online]. Available: https://ieeexplore.ieee.org/document/1036195/.

[56] M. Yu, C. Kan, M. Lewis, and A. Sizmann, "Statistics of signal-to-noise ratio and path-accumulated power due to concatenation of polarization-dependent loss," *IEEE Photonics Technology Letters*, vol. 14, no. 10, pp. 1418–1420, Oct. 2002, ISSN: 1941-0174. DOI: 10.1109/LPT.2002.802384. Accessed: Jul. 28, 2026. [Online]. Available: https://ieeexplore.ieee.org/document/1037536/.

[57] A. Mecozzi and M. Shtaif, "Signal-to-noise-ratio degradation caused by polarization-dependent loss and the effect of dynamic gain equalization," *Journal of Lightwave Technology*, vol. 22, no. 8, pp. 1856–1871, Aug. 2004, ISSN: 1558-2213. DOI: 10.1109/JLT.2004.832424. Accessed: Jul. 28, 2026. [Online]. Available: https://ieeexplore.ieee.org/document/1321182.

[58] C. Xie, "Polarization-dependent loss-induced outage probabilities in optical communication systems," *IEEE Photonics Technology Letters*, vol. 20, no. 13, pp. 1091–1093, Jul. 2008, ISSN: 1941-0174. DOI: 10.1109/LPT.2008.924298. Accessed: Jul. 28, 2026.

This work is licensed under a Creative Commons Attribution 4.0 License. For more information, see https://creativecommons.org/licenses/by/4.0/

This article has been accepted for publication in IEEE Open Journal of the Communications Society. This is the author's version which has not been fully edited and content may change prior to final publication. Citation information: DOI 10.1109/OJCOMS.2026.3741461

[Online]. Available: https://ieeexplore.ieee.org/document/4531630.

[59] L. Dou, Z. Tao, T. Hoshida, and J. C. Rasmussen, "Analysis of polarization dependent loss impact on optically amplified multi-span dual-polarization systems," in *2011 IEEE International Conference on Communications (ICC)*, ISSN: 1938-1883, Jun. 2011, pp. 1–6. DOI: 10.1109/icc.2011.5962748. Accessed: Jul. 28, 2026. [Online]. Available: https://ieeexplore.ieee.org/document/5962748.

[60] T. Sun, N. Cui, C. Ji, J. Zhao, X. Zhang, and L. Xi, "Equivalent relationship between lumped model and distributed model of PDL based on SNR penalty," in *2023 Opto-Electronics and Communications Conference (OECC)*, ISSN: 2166-8892, Jul. 2023, pp. 1–3. DOI: 10.1109/OECC56963.2023.10209742. Accessed: Jul. 28, 2026. [Online]. Available: https://ieeexplore.ieee.org/document/10209742/.

[61] J. Zhou, T. Liu, and Y. Wang, "Exact noise statistics in equalized polarization multiplexing systems in the presence of polarization dependent loss," *Journal of Lightwave Technology*, vol. 41, no. 16, pp. 5366–5372, Aug. 2023, ISSN: 1558-2213. DOI: 10.1109/JLT.2023.3262939. Accessed: Jul. 28, 2026. [Online]. Available: https://ieeexplore.ieee.org/document/10086575/.

[62] J. C. Cartledge and A. I. A. El-Rahman, "Impact of transceiver noise on the outage probability due to polarization dependent loss," *IEEE Photonics Technology Letters*, vol. 33, no. 1, pp. 59–62, Jan. 2021, ISSN: 1941-0174. DOI: 10.1109/LPT.2020.3043119. Accessed: Jul. 28, 2026. [Online]. Available: https://ieeexplore.ieee.org/document/9285304/.

[63] N. Rossi, B. Lavigne, P. Serena, and C. Lasagni, "Deterministic yet stochastic approach to model PDL-impaired SNR performance of coherent optics," in *2024 IEEE Opto-Electronics and Communications Conference (OECC)*, ISSN: 2166-8892, Jun. 2024, pp. 1–3. DOI: 10.1109/OECC54135.2024.10975438. Accessed: Jul. 28, 2026. [Online]. Available: https://ieeexplore.ieee.org/document/10975438/.

[64] A. D'Amico et al., "Disaggregated statistical characterization of the PDL impairment on the optical signal-to-noise ratio," in *2023 International Conference on Photonics in Switching and Computing (PSC)*, Mantova, Italy: IEEE, Sep. 26, 2023, pp. 1–3, ISBN: 979-8-3503-2370-2. DOI: 10.1109/PSC57974.2023.10297261. Accessed: Jul. 23, 2026. [Online]. Available: https://ieeexplore.ieee.org/document/10297261/.

[65] N. Rossi, P. Serena, and A. Bononi, "Polarization-dependent loss impact on coherent optical systems in presence of fiber nonlinearity," *IEEE Photonics Technology Letters*, vol. 26, no. 4, pp. 334–337, Feb. 2014, ISSN: 1941-0174. DOI: 10.1109/LPT.2013.2293595. Accessed: Jul. 28, 2026. [Online]. Available: https://ieeexplore.ieee.org/document/6678178.

[66] P. Serena, S. Musetti, S. Almonacil, S. Bigo, Benoni, and P. Jennevé. "The gaussian noise model extended to polarization dependent loss and its application to outage probability estimation," Accessed: Jul. 28, 2026. [Online]. Available: https://ieeexplore.ieee.org/document/8535569.

[67] N. Rossi, S. Musetti, P. Ramantanis, and S. Almonacil, "The impact of kerr nonlinearity on the SNR variability induced by polarization-dependent loss," *Journal of Lightwave Technology*, vol. 37, no. 19, pp. 5048–5055, Oct. 2019, ISSN: 1558-2213. DOI: 10.1109/JLT.2019.2927407. Accessed: Jul. 28, 2026. [Online]. Available: https://ieeexplore.ieee.org/document/8769939.

[68] J. Zhou, Y. Wang, and T. Liu, "Analytical formulation of fiber nonlinear noise statistics in the presence of polarization dependent loss," *Journal of Lightwave Technology*, vol. 42, no. 2, pp. 681–688, Jan. 2024, ISSN: 1558-2213. DOI: 10.1109/JLT.2023.3314614. Accessed: Jul. 28, 2026. [Online]. Available: https://ieeexplore.ieee.org/document/10247521/.

[69] A. Rosso, E. Miotto, E. Virgillito, S. Straullu, and V. Curri, "Is the gaussian channel model suitable for converged metro-access optical networks?" In *2025 25th Anniversary International Conference on Transparent Optical Networks (ICTON)*, 2025, pp. 1–4. DOI: 10.1109/ICTON67126.2025.11125300.

[70] A. Nafta and M. Shtaif, "The ultimate cost of PDL in fiber-optic systems," in *2009 Conference on Lasers and Electro-Optics and 2009 Conference on Quantum electronics and Laser Science Conference*, ISSN: 2160-9004, Jun. 2009, pp. 1–2. DOI: 10.1364/CLEO.2009.CMC2. Accessed: Jul. 28, 2026. [Online]. Available: https://ieeexplore.ieee.org/document/5225757/.

[71] C. Xie, "Polarization-dependent loss induced penalties in PDM-QPSK coherent optical communication systems," in *2010 Conference on Optical Fiber Communication (OFC/NFOEC), collocated National Fiber Optic Engineers Conference*, Mar. 2010, pp. 1–3. Accessed: Jul. 28, 2026. [Online]. Available: https://ieeexplore.ieee.org/document/5465573/.

[72] E. Miotto et al., "Closed-form statistical modeling of PDL-induced SNR margins for reliable optical networks," 2026.

[73] N. Rossi, T. Zami, and B. Lavigne, "Impact of statistical LCoS-induced PDL in WDM networks equipped with multirail amplifiers and 800ZR+ interfaces," in *European Conference on Optical Communication (ECOC)*, Accepted for publication, 2026.

[74] A. N. Kolmogorov, "Sulla determinazione empirica di una legge di distribuzione," *Giornale dell'Istituto Italiano degli Attuari*, vol. 4, pp. 83–91, 1933.

[75] N. Smirnov, "Table for estimating the goodness of fit of empirical distributions," *The Annals of Mathemati-*

This work is licensed under a Creative Commons Attribution 4.0 License. For more information, see https://creativecommons.org/licenses/by/4.0/

This article has been accepted for publication in IEEE Open Journal of the Communications Society. This is the author's version which has not been fully edited and content may change prior to final publication. Citation information: DOI 10.1109/OJCOMS.2026.3741461

cal Statistics, vol. 19, no. 2, pp. 279–281, 1948. DOI: 10.1214/aoms/1177730256.

[76] F. J. Massey, "The Kolmogorov-Smirnov test for goodness of fit," *Journal of the American Statistical Association*, vol. 46, no. 253, pp. 68–78, 1951. DOI: 10.1080/01621459.1951.10500769.

[77] T. Chai and R. R. Draxler, "Root mean square error (RMSE) or mean absolute error (MAE)? arguments against avoiding RMSE in the literature," *Geoscientific Model Development*, vol. 7, no. 3, pp. 1247–1250, 2014. DOI: 10.5194/gmd-7-1247-2014.

[78] S. Kullback and R. A. Leibler, "On information and sufficiency," *The Annals of Mathematical Statistics*, vol. 22, no. 1, pp. 79–86, 1951. DOI: 10.1214/aoms/1177729694.

[79] R. Koenker, *Quantile Regression* (Econometric Society Monographs). Cambridge, U.K.: Cambridge University Press, 2005, vol. 38. DOI: 10 . 1017 / CBO9780511754098.

[80] A. J. McNeil, R. Frey, and P. Embrechts, *Quantitative Risk Management: Concepts, Techniques and Tools*, Revised. Princeton, NJ, USA: Princeton University Press, 2015.



ENRICO MIOTTO (Graduate Student Member, IEEE) is a Ph.D. student with the Open PLANET Lab research group at the Department of Electronics and Telecommunications of Politecnico di Torino, Italy. He received his B.Sc. degree summa cum laude in Information Engineering from Università degli Studi di Padova in 2022. He moved to Politecnico di Torino to pursue an M.Sc. degree in Communications Engineering, specializing in optical-fiber communications, and graduated summa cum laude in 2024. His research interests encompass optical networking, with a focus on mathematical and physical electromagnetic modeling applied to optical communications. His recent publications address system-margin assessment of filtering penalties and polarization-dependent loss due to wavelength-selective switches, specifically with regard to quality-of-transmission estimation for the development of an optical network digital twin. He is a student member of Optica and an active member of the Optica student chapter in Turin.



GIORGIO TARICCO(M'91–SM'03–F'10) received his *Laurea in Ingegneria Elettronica* (*cum laude*) from Politecnico di Torino (Italy) in 1985. He was a researcher at CSELT (Italian Telecom Labs) from 1985 to 1987, during which time he was involved in the design process of the GSM mobile telephony standard (channel coding). Since 1991, he has been with the Department of Electronics and Telecommunications (DET) at Politecnico di Torino, first as an Assistant Professor and, since 2010, as a Full Professor. In 1996, he was a Research Fellow at ESA/ESTEC, The Netherlands. He participated in several IEEE conference committees as Treasurer and has been an Associate Editor of the *IEEE Communications Letters*, the *IEEE Transactions on Information Theory*, the *Journal on Communications and Networks*, and a Senior Associate Editor for the *IEEE Wireless Communications Letters*. He is currently a Section Board Member of *MDPI Entropy*.

His research interests include information theory, error-control coding, multiuser detection, space-time coding, MIMO communications, cognitive radio networks, sensor networks, IoT satellite networks, MIMO relay channels, NOMA communications, FSO communications, ISAC systems, and bandit algorithms. He has co-authored more than two hundred papers published in international journals and conference proceedings, several book chapters, and three international patents. He was a co-recipient of Best Paper Awards at the WPMC 2001 conference and from the *Journal of Communications and Networks (Special Issue on Coding and Signal Processing for MIMO Systems)* (2003). He was included in the ISI Highly Cited Researchers list in the Computer Science category from 2008 to 2013.



HIDEKI NISHIZAWA is a Senior Research Engineer at NTT Network Innovation Laboratories, NTT Corporation, Japan. He received the B.S. and M.S. degrees in Physics from Chiba University, Japan, in 1994 and 1996, respectively. He joined NTT Laboratories in 1996, where he has been engaged in research and development of open and disaggregated optical networking technologies and Optical Network Digital Twins (ONDTs). He also serves as the Coordinator of the Open APN Task Force in the Innovative Optical and Wireless Network (IOWN) Global Forum and Co-Leader of the Disaggregated Optical Systems (DOS) Subgroup in the Telecom Infra Project (TIP) Open Optical and Packet Transport (OOPT) Project Group. He received the Ph.D. degree in Information Science and Technology from Hokkaido University, Japan, in 2025. He is a Senior Member of the IEEE. His current research interests include open optical networking, Optical Network Digital Twins, AI-assisted optical network operations, and multi-vendor interoperability.



ANDREA D'AMICOis a researcher at NEC Laboratories America, Princeton, USA. He received the B.S. and M.S. degrees in Physics from Università di Pisa in 2012 and 2016, and he obtained his Ph.D. in Electric, Electronic and Communication Engineering from Politecnico di Torino in 2023. He worked as a software engineer at NTT Data in Milan on big-data projects in 2018. He joined NEC Laboratories America in 2023 to conduct research on optical communications and networking, focusing on optical transmission and optical network digital twins. He is currently the co-leader of the PSE group in the Telecom Infra Project and co-maintainer of the open-source library GNPy.

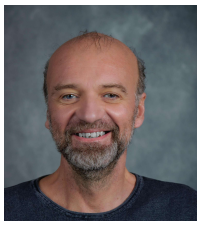

VITTORIO CURRI (Fellow, IEEE) received the Laurea degree in electrical engineering cum laude in 1995, and the Scientific Doctoral degree in optical communications in 1999, both from Politecnico di Torino (PoliTO), Italy. He is a founding member of the OptCom group and PhotonLab at PoliTO and currently leads the Open PLANET Lab. He is a Full Professor in the Department of Electronics and Telecommunications at PoliTO. He has been a visiting scholar at Stanford University and the University of California, Santa Barbara. His major research interests are in fiber transmission modeling, including nonlinearities, transmitter and receiver optimization, design strategies for optical links, Raman amplification, and the simulation and modeling of optical communication systems. Prof. Curri was among the early promoters of multiband transmission in single-mode fibers and is also active in analyzing the impact of the physical layer on the planning and control of open and disaggregated optical networks based on vendor-neutral digital twins, including AI techniques. He is the Scientific Chair of the GNPy open-source project within the industry consortium Telecom Infra Project. He was also an early promoter of using the optical network as a sensor. Prof. Curri is an IEEE Fellow, an Optica Fellow, and an AAIA Fellow, and is the co-author of more than 600 scientific publications.

This work is licensed under a Creative Commons Attribution 4.0 License. For more information, see https://creativecommons.org/licenses/by/4.0/